Supplement of Atmos. Chem. Phys., 25, 16127–16145, 2025 https://doi.org/10.5194/acp-25-16127-2025-supplement © Author(s) 2025. CC BY 4.0 License.





Supplement of

Elemental composition, iron mineralogy, and solubility of anthropogenic and natural mineral dust aerosols in Namibia: a case study analysis from the AEROCLO-sA campaign – Part 2

Paola Formenti et al.

Correspondence to: Paola Formenti (paola.formenti@lisa.ipsl.fr)

The copyright of individual parts of the supplement might differ from the article licence.

Table S1. Ancillary instrumentation relevant to this publication

Observables	Instrumentation	Details of sampling	Frequency of acquisition	
Wind speed/ direction, air temperature, relative humidity	Compact weather station (model CE155N, CE157N, BA711, Cimel Electronique, Paris, France)	10 m above ground level, extendable mast on the roof of the PEGASUS facility.	5-minute	
Particle number size distribution (0.25-32 µm optical diameter)	Optical particle counter (OPC, model 1.109, GRIMM Inc., DE)	Flow rate = 1.2 L min ⁻¹	6-sec resolution	

Table S2. List of standard material and reference spectra used for the least-square deconvolution of the XANES spectra. The first four lines report the identification numbers and details of preparation of the six standards that were prepared for these work. They consisted of as round pellets of 10 mm² in a matrix of Boron Nitride (BN, molar mass 24.819 g mol¹) prepared using an automatic hydraulic Press (Atlas Power T8, Specac), available at the chemistry laboratory at SOLEIL, operated at a pressure of 5 Tons. The dilution rate of the standard compounds was adjusted using the ABSORBIX (X-ray absorbance and fluorescence self-absorption calculations) software to optimize the absolute and relative values of the Fe-absorption edge (Michalowicz et al., 2009). The Fe mass and total pellet mass are reported in the last column (the total pellet mass is in brackets). The pellets were analyzed sequentially in transmission mode.

ID	CAS number	Stoichiometric formula	Dilution rate in the pellet (%)	Total surface mass concentration (g cm ⁻²)	Mass of standard, μg
Ref4	13268-42-3	(NH ₄) ₃ [Fe(C ₂ O ₄) ₃] 3H ₂ O	20	0.125	19.75 (97.5)
Ref6	166897-40-1	Fe ₂ (C ₂ O ₄) ₃ 6H ₂ O	12	0.125	11.70 (97.5)
Ref1	6047-25-2	$Fe \cdot (C_2O_4) \cdot 2(H_2O)$	10	0.125	9.75 (97.5)
Ref15	1345-25-1	FeO	5	0.110	4.29 (97.5)

Table S3. Summary statistics of elemental and water-soluble ionic concentrations measured during the campaign in the TSP and PM_1 fractions. The second column indicates the number of samples for which values were above the minimum quantification limit (MQL). The arithmetic means and standard deviations (SD) are reported in ng m⁻³. The MQL values in ng m-3 are calculated from the concentrations measured on the analytical blanks using the average sampling volume during the whole campaign and its standard deviation. NA (=not applicable) indicates instances for which the element was below MQL. ND (=not determined) indicates that the element was not measured. For compounds determined by ion chromatography (indicated by an asterisk in the table) the MQL are reported in mg L⁻¹.

		TSP			PM₁	
	Mean	SD	Number of samples	Mean	Std	Number of samples
CI	37338	18647	36	1070	721	28
S	3069	1359	36	429	146	28
Ca	1744	771	36	94	70	28
Fe	582	412	36	38	39	23
Na	22829	11169	36	611	360	28
Mg	2812	1284	36	89	48	28
Al	582	426	36	30	27	28
Si	2575	1448	36	208	83	28
Р	18	8	36	$< 0.3 \pm 0.1$	NA	NA
K	1254	550	36	52	25	28
Ti	57	41	36	4	3	23
Mn	15	11	36	10	12	17
Zn	13	7	36	ND	ND	ND
Cr	7	4	34	ND	ND	ND
V	11	5	36	ND	ND	ND
Ва	6	5	7	ND	ND	ND
Co	8	4	36	ND	ND	ND
Cu	13	5	36	ND	ND	ND
Nd	13	6	36	ND	ND	ND
Ni	10	5	36	ND	ND	ND
Sr	54	30	35	ND	ND	ND
Cd	197	156	25	ND	ND	ND
As	74	52	34	ND	ND	ND
Pb	40	30	35	ND	ND	ND
Na⁺	22155	10743	35	819	414	28
K ⁺	1184	618	35	56	21	25
Ca²+	1658	750	35	62	18	17
Mg²+	3679	2012	35	89	45	26
CI ⁻	38894	20550	35	906	620	28
SO ₄ 2-	9066	4272	35	1083	352	28
NH ₄ +	260	128	35	239	83	28
MSA	61	26	25	46	16	25
NO₃⁻	965	687	35	100	29	28
F-	4330	2317	13	301	166	28
Br⁻	170	154	27	< 0.02*	NA	NA
PO ₄ ³-	39	12	4	< 0.01*	NA	NA
oxalate	125	50	27	69	19	28
formate	405	274	23	18	5	11
acetate	32	11	9	20	9	27

ОС	3213	1459	36	117	57	28
EC	271	234	28	14	9	9

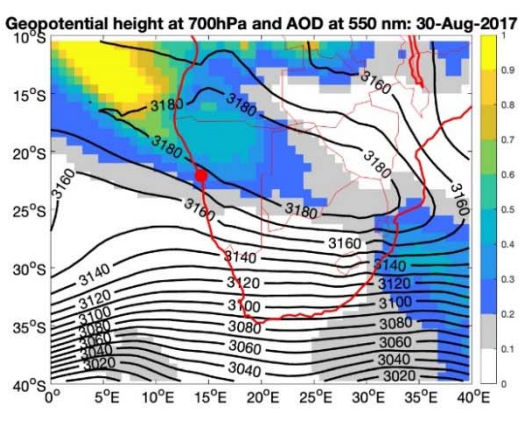
$\textbf{Table S4.} \ \textbf{The list of AI}_{\text{con}}\textbf{-}\textbf{based formulae classes with atomic constraints}$

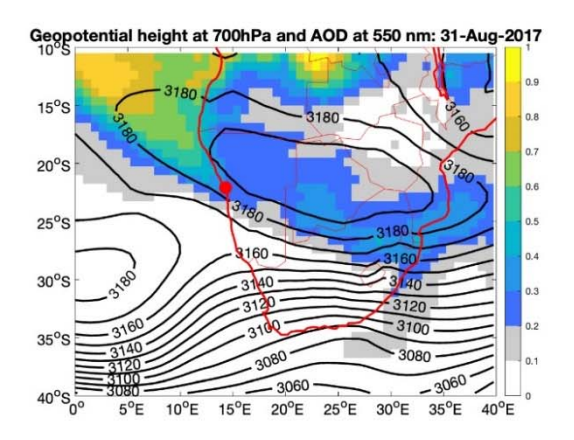
Formulae class	O/C	H/C	Alcon
Lipids	< 0.3	≥ 1.5**	-
N-containing saturated compounds (N-saturated)	-	≥ 1.5*	-
Aliphatics	≥ 0.3	≥ 1.5**	-
Unsaturated (low O/C)	< 0.5	< 1.5	< 0.5
Unsaturated (high O/C)	≥ 0.5	< 1.5	< 0.5
Aromatic (low O/C)	< 0.5	-	≥ 0.5 and < 0.67
Aromatic (high O/Ć)	≥ 0.5	-	≥ 0.5 and < 0.67
Condensed (low O/C)	< 0.5	-	≥ 0.67
Condensed (high O/C)	≥ 0.5	-	≥ 0.67

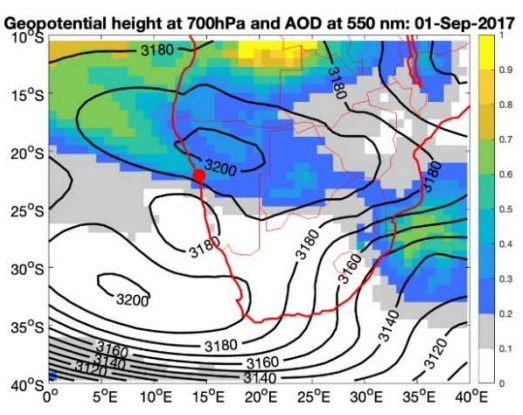
50 * N > 0; ** N = 0

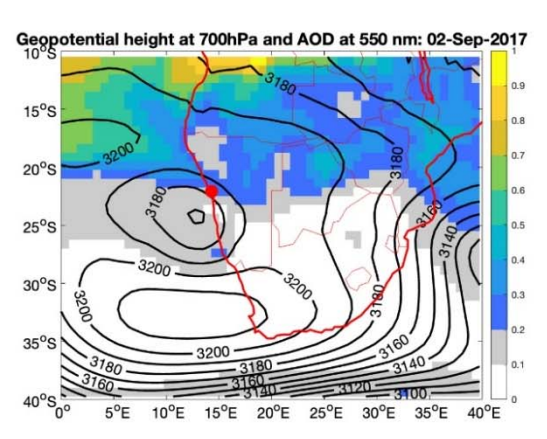
48

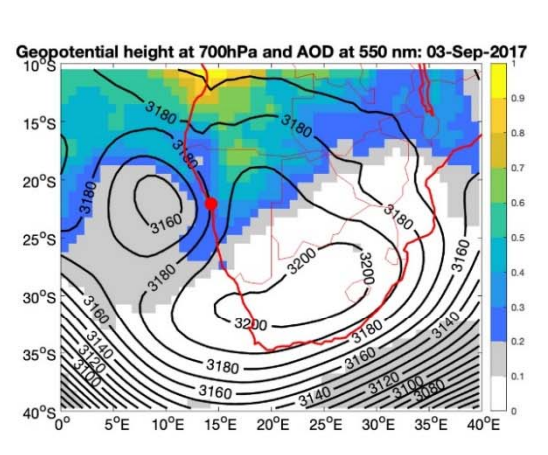
49

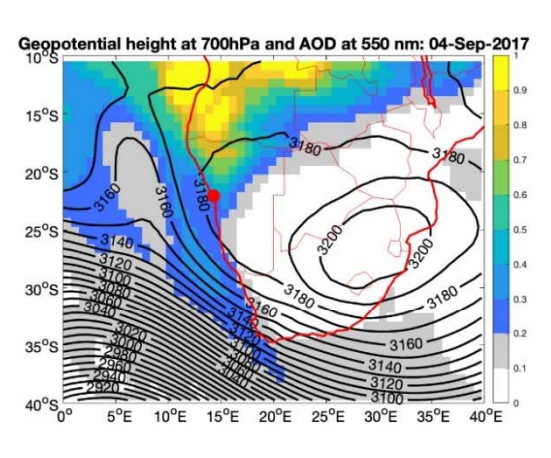


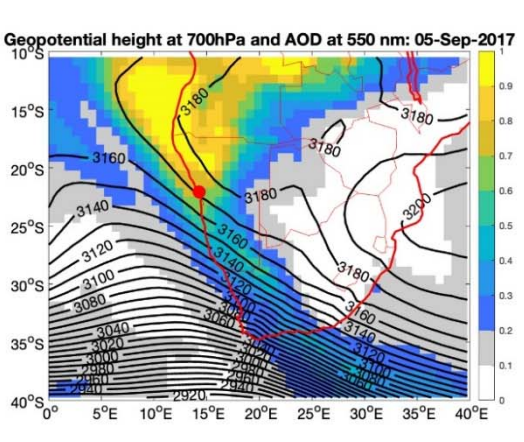


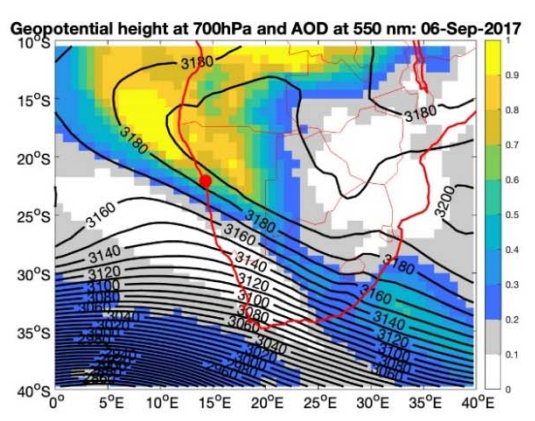


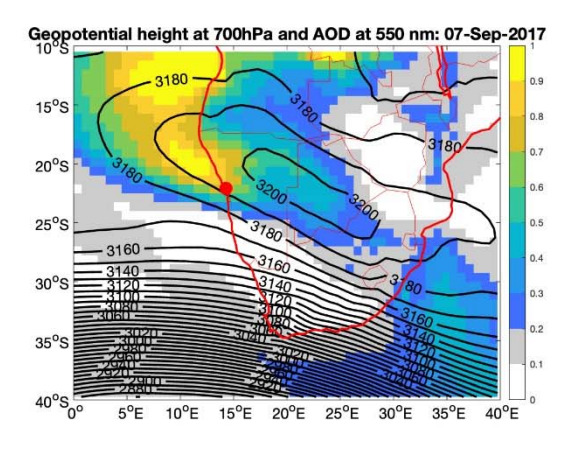


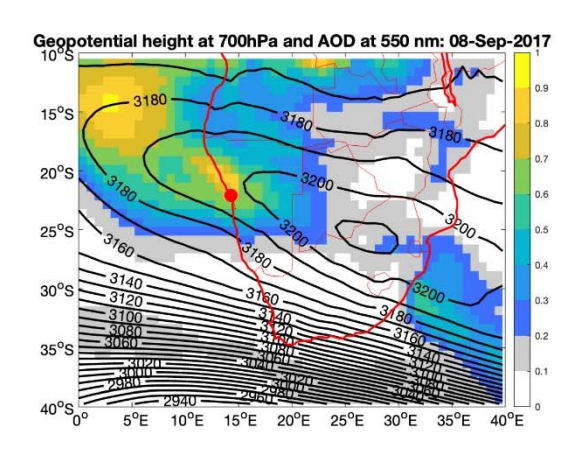


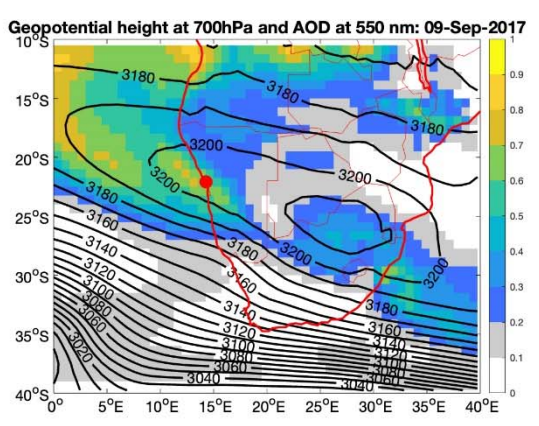


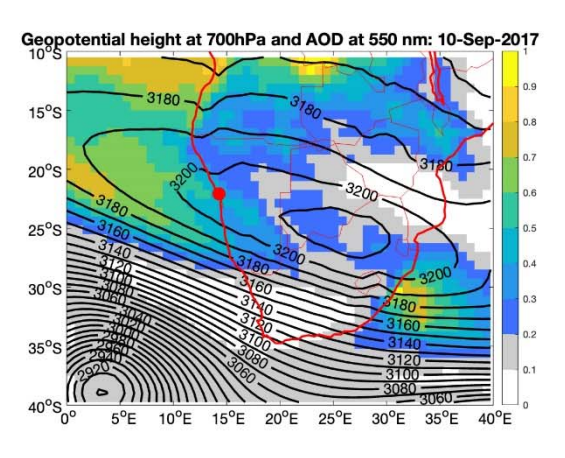


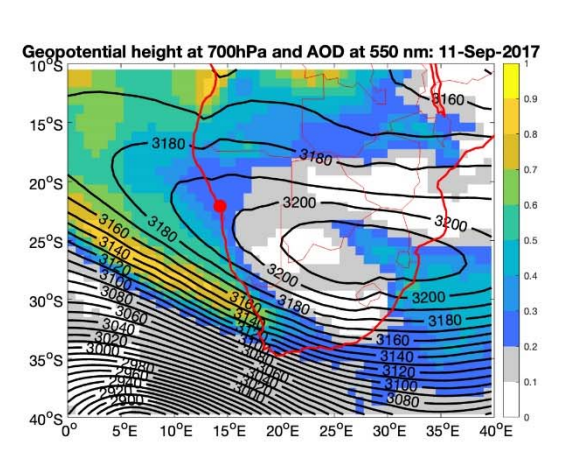












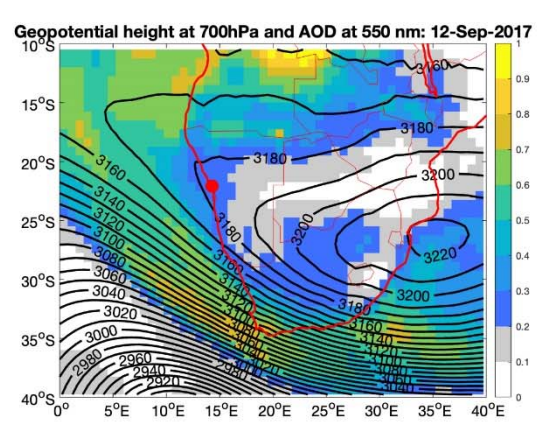
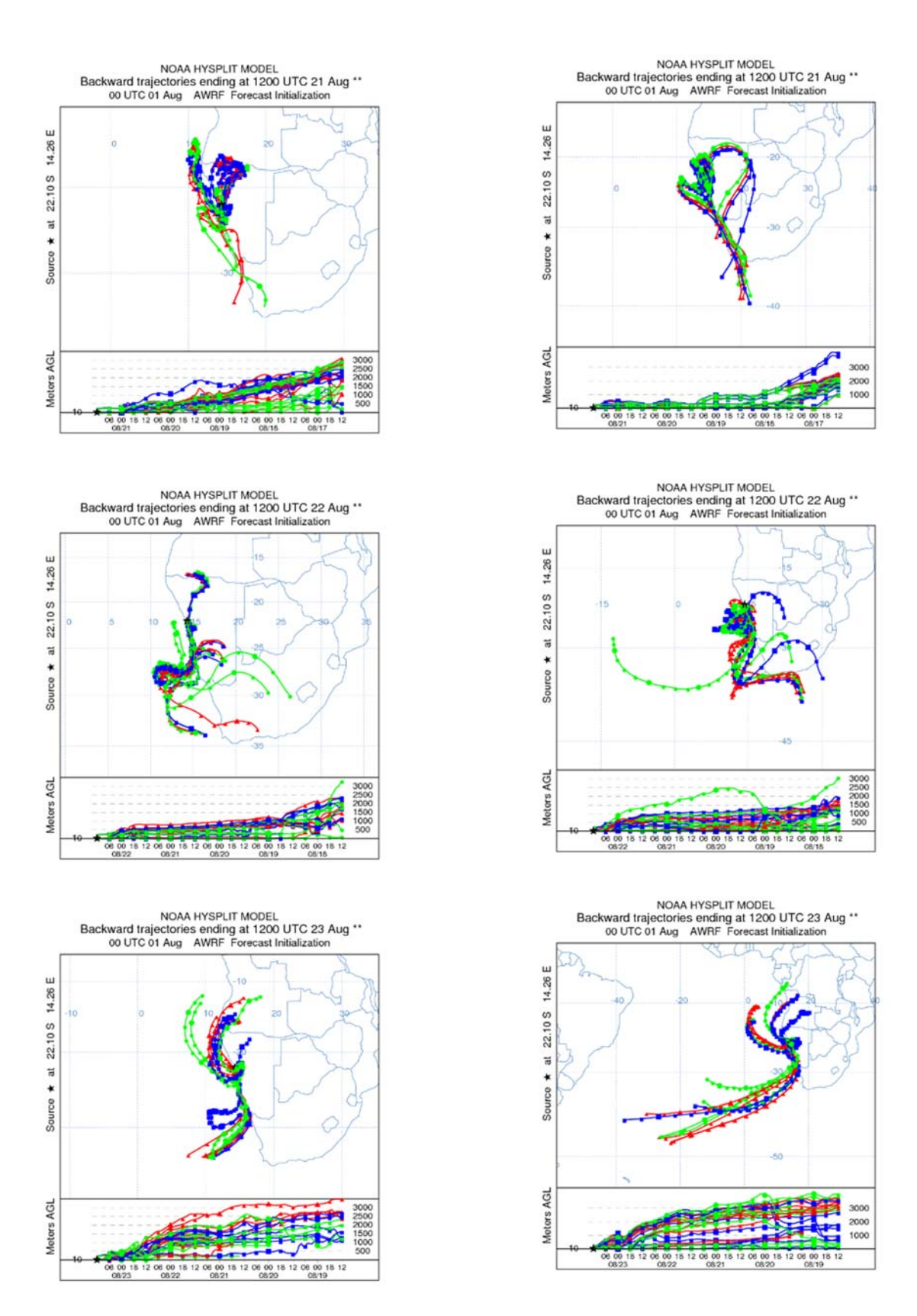
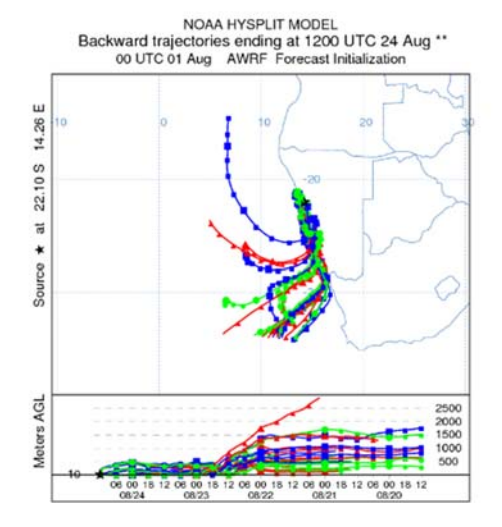
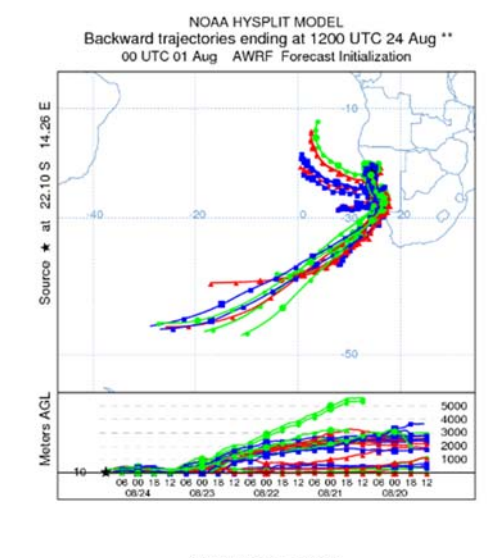
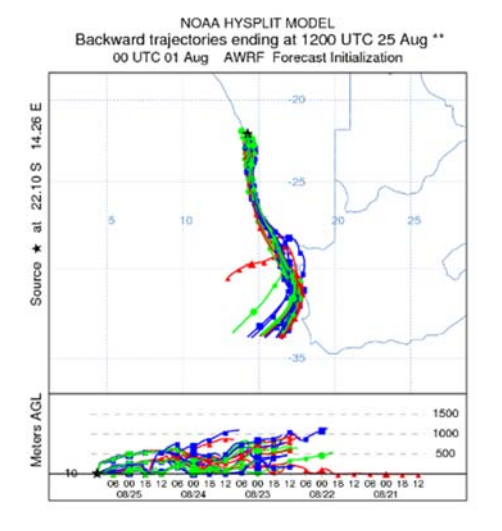


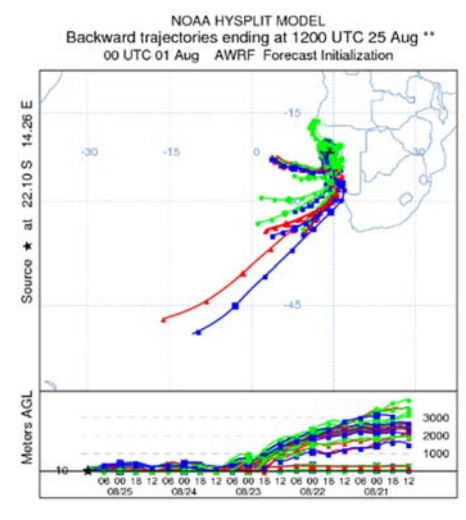
Figure S3. Air mass back-trajectories calculated with 9 km (left) and 50 km (right) spatial resolution

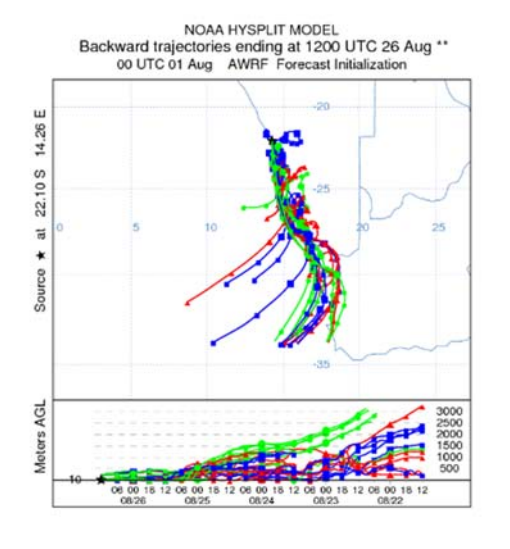


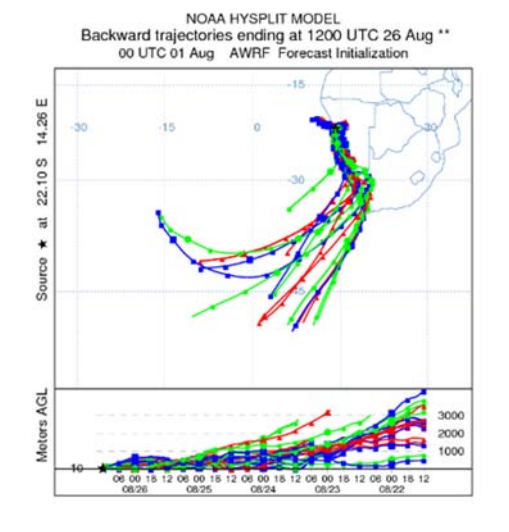


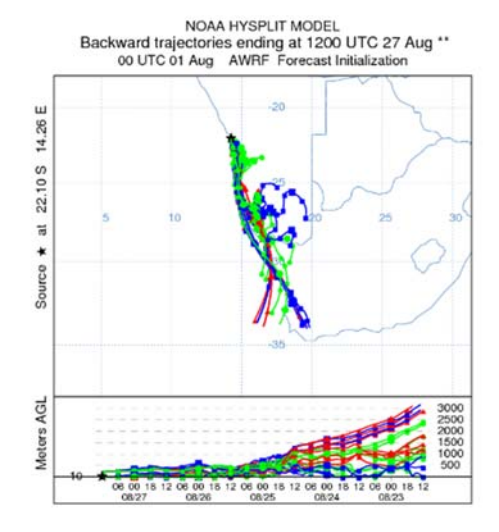


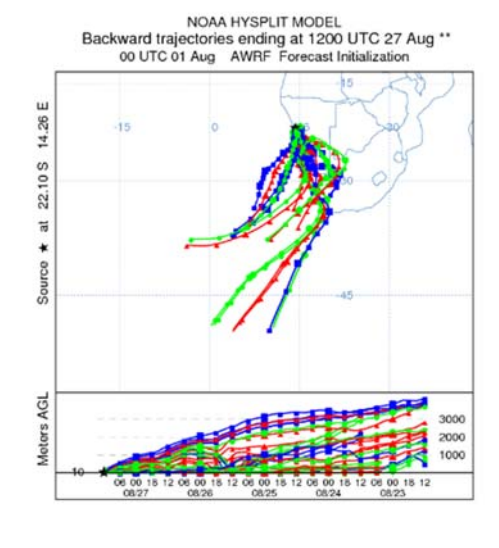


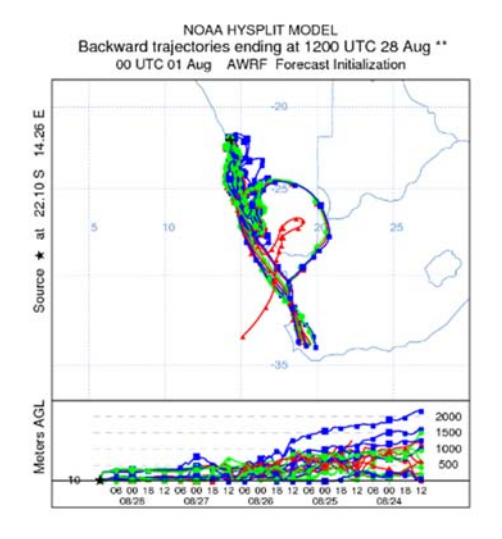


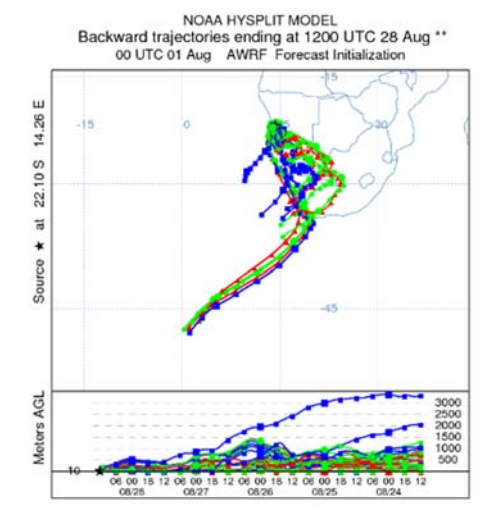


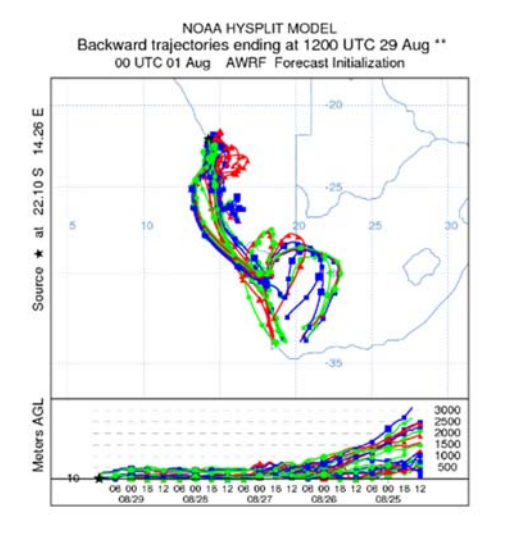


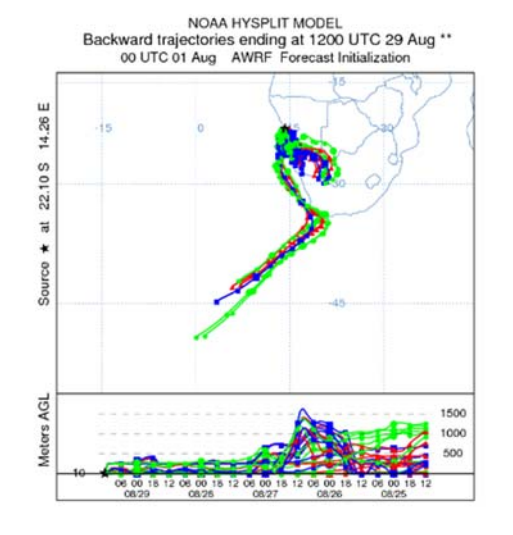


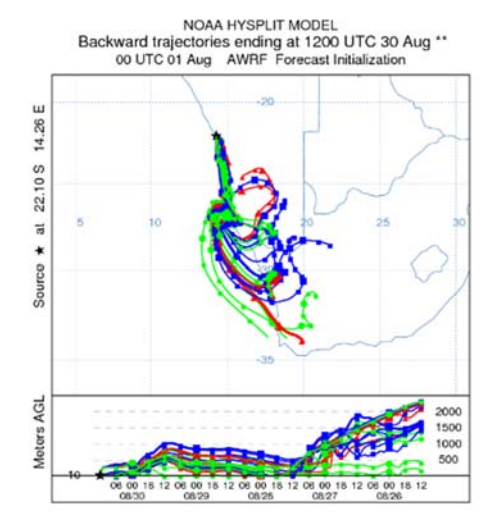


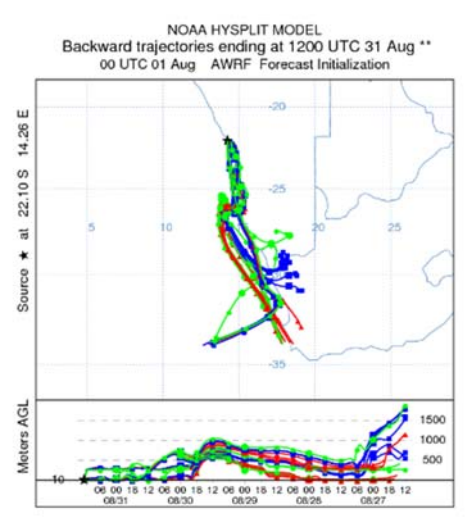


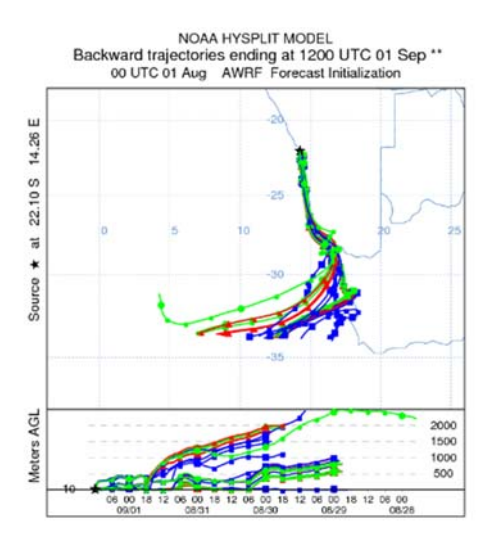


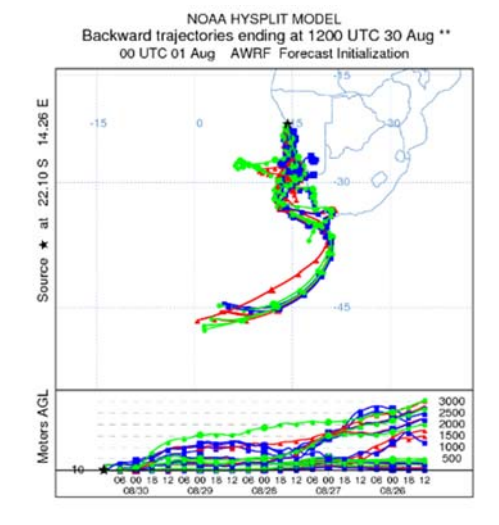


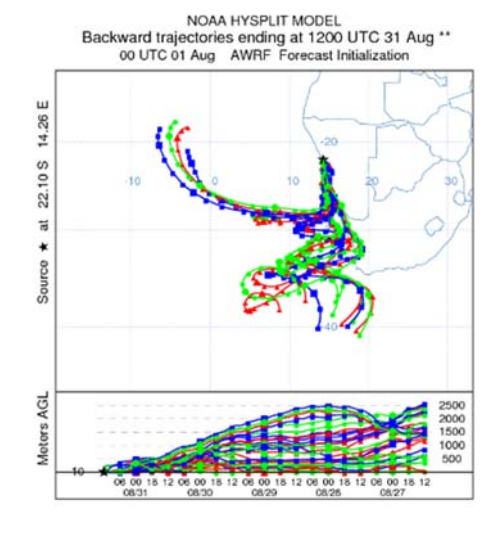


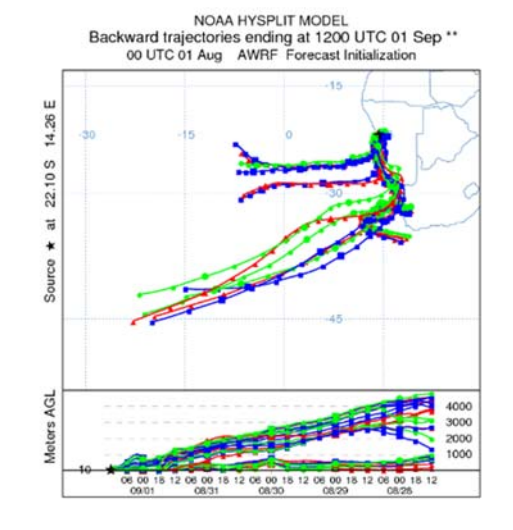


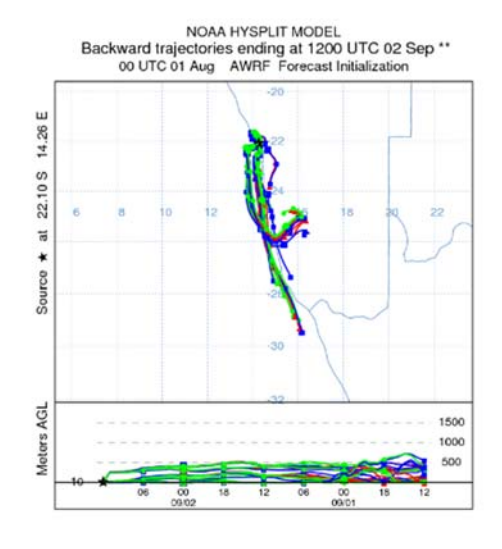


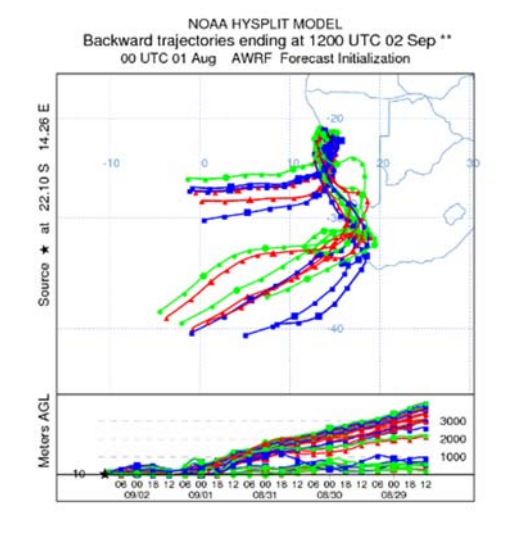


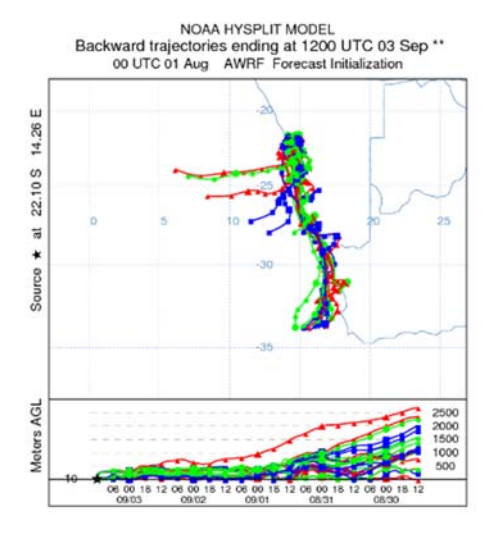


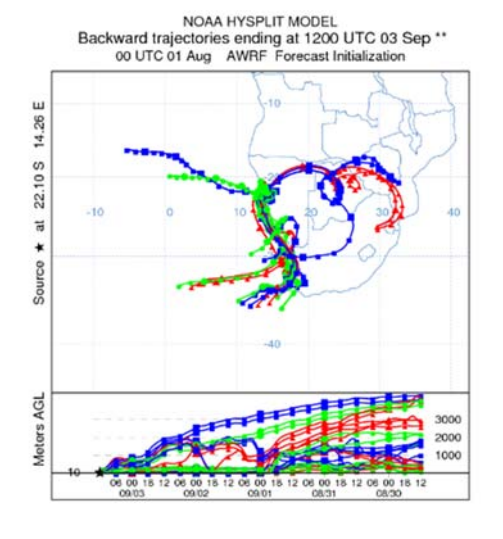


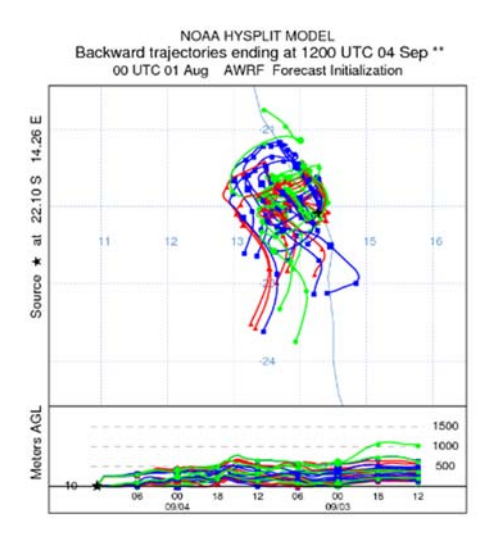


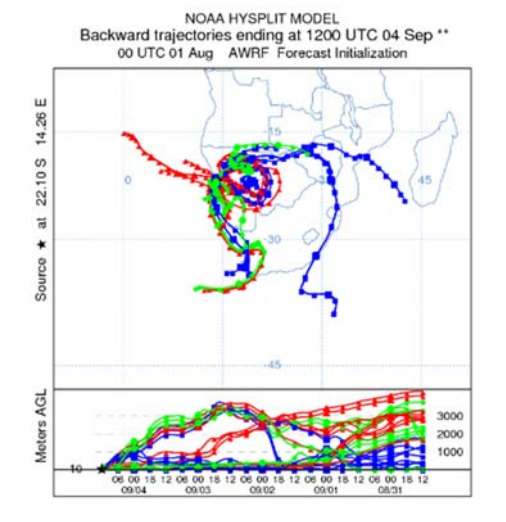


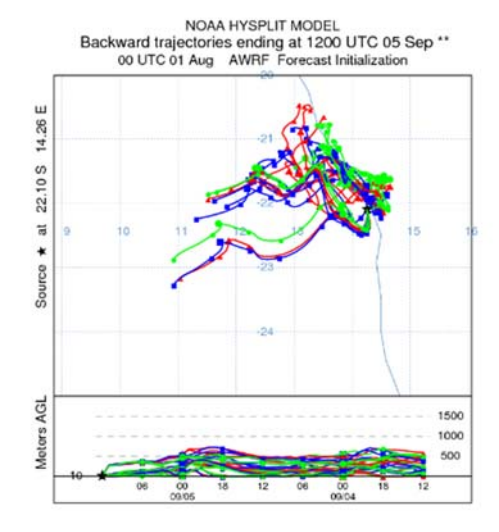


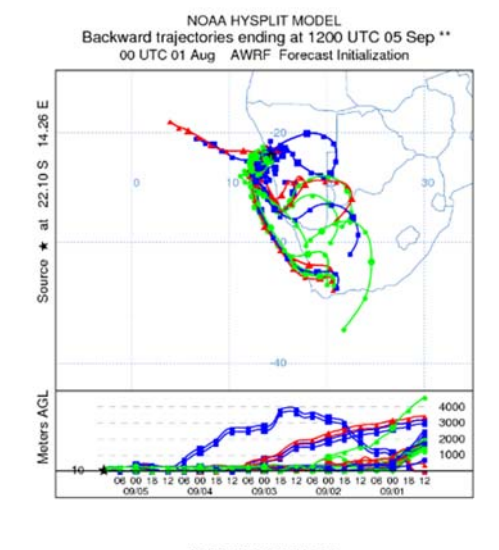


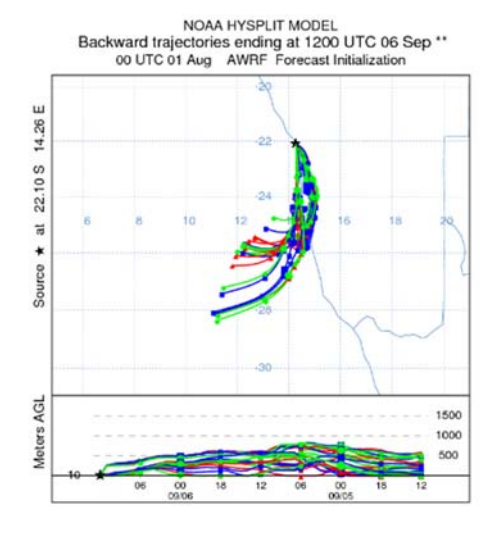


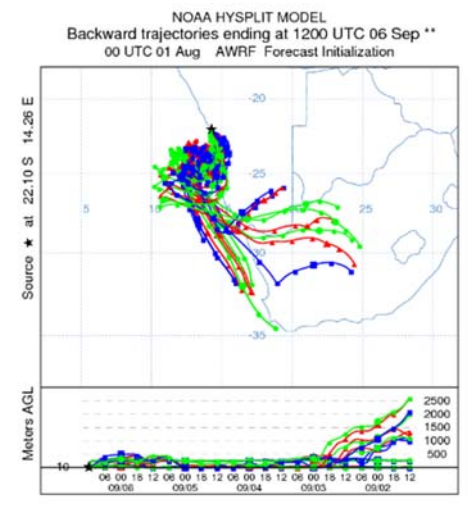


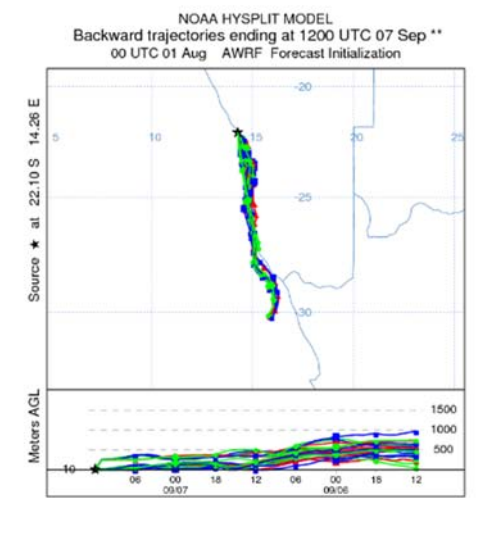


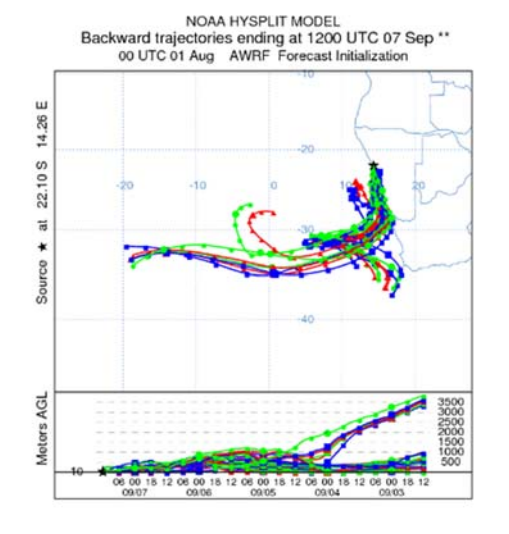


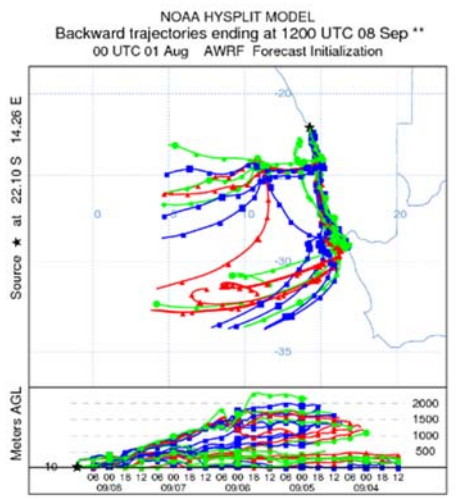


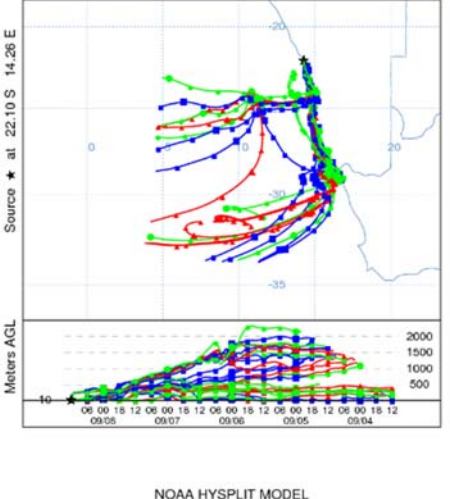


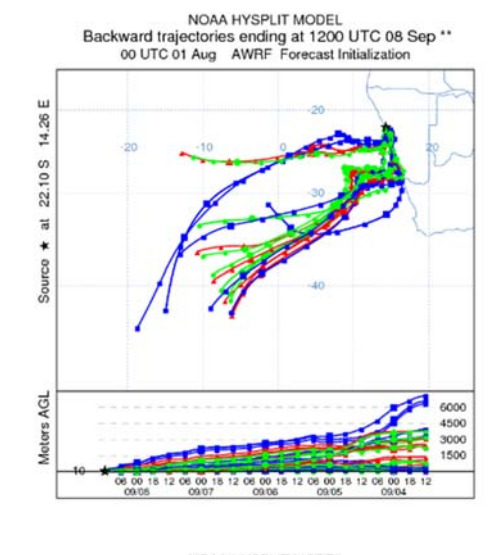


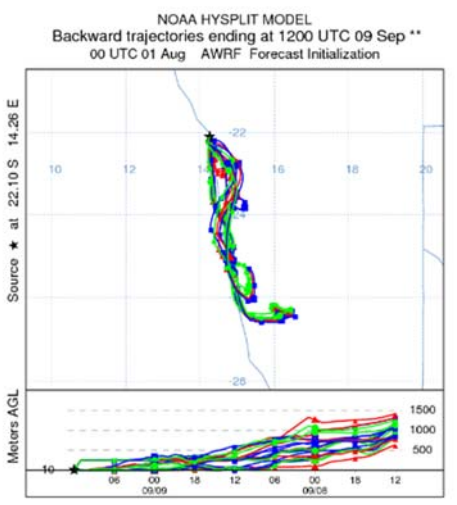


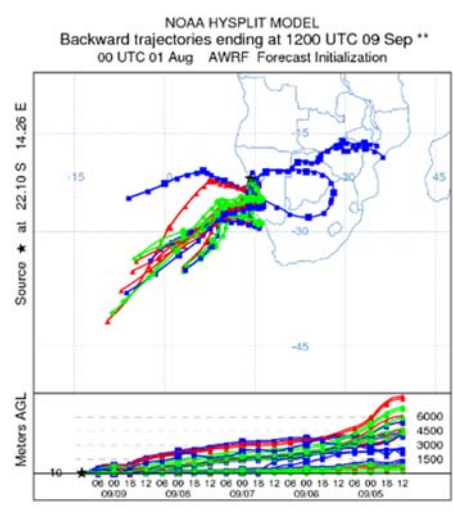


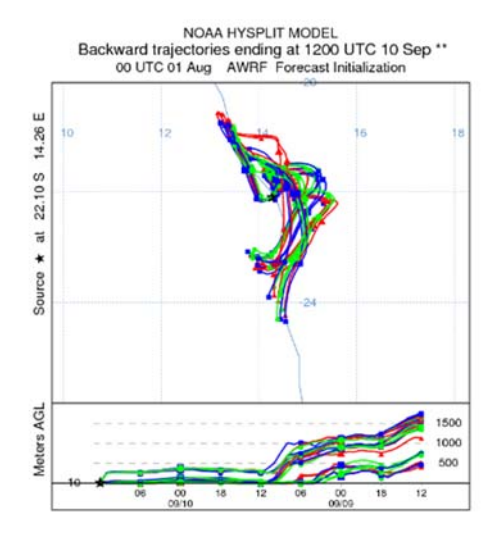


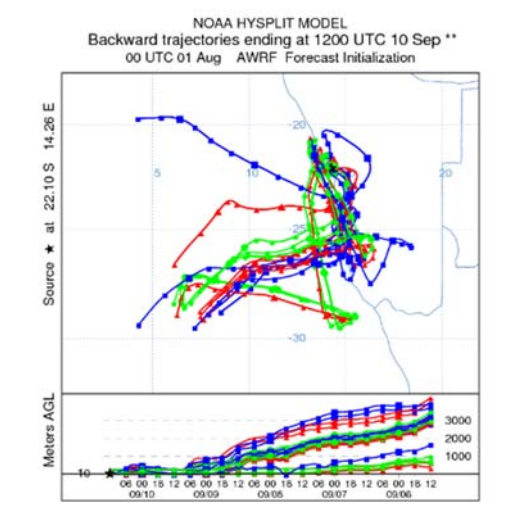


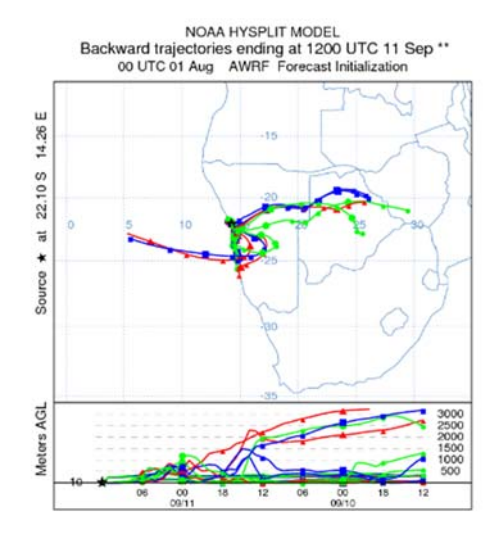


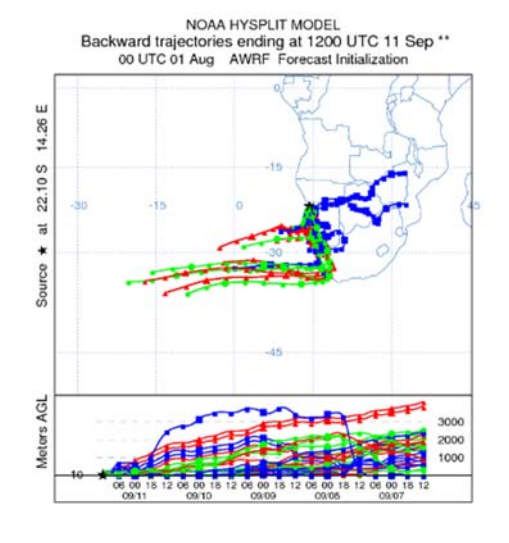


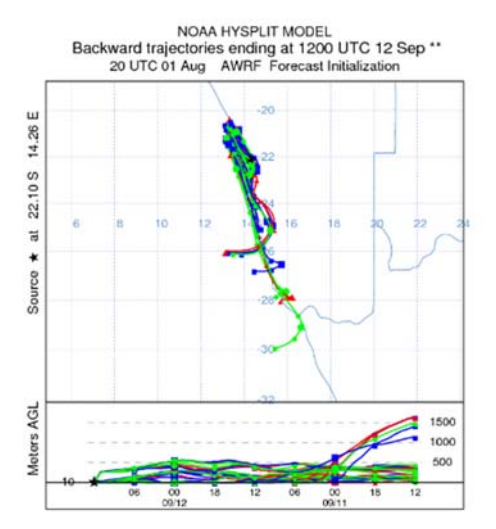


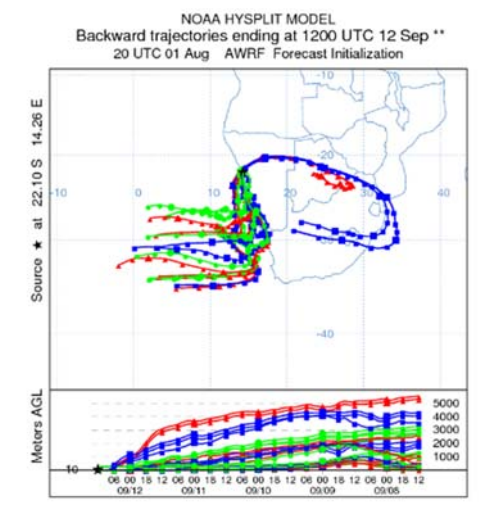












69

70

71

72

73

74

Figure S5. Box and whiskers distributions of ratios to Al of various elements measured during the field campaign. Values are sorted according to the meteorological periods P1 to P3. The P3 period is split into two sub-periods (P3a and P3b) to highlight the changes in the particle composition towards the end of the campaign. The box indicates the interquartile range, i.e. the 25th and 75th percentiles, and the line within the box marks the median. The whiskers indicate the quartiles 1.5 times the interquartile range. Points above and below the whiskers indicate outliers outside the 10th and 90th percentiles.

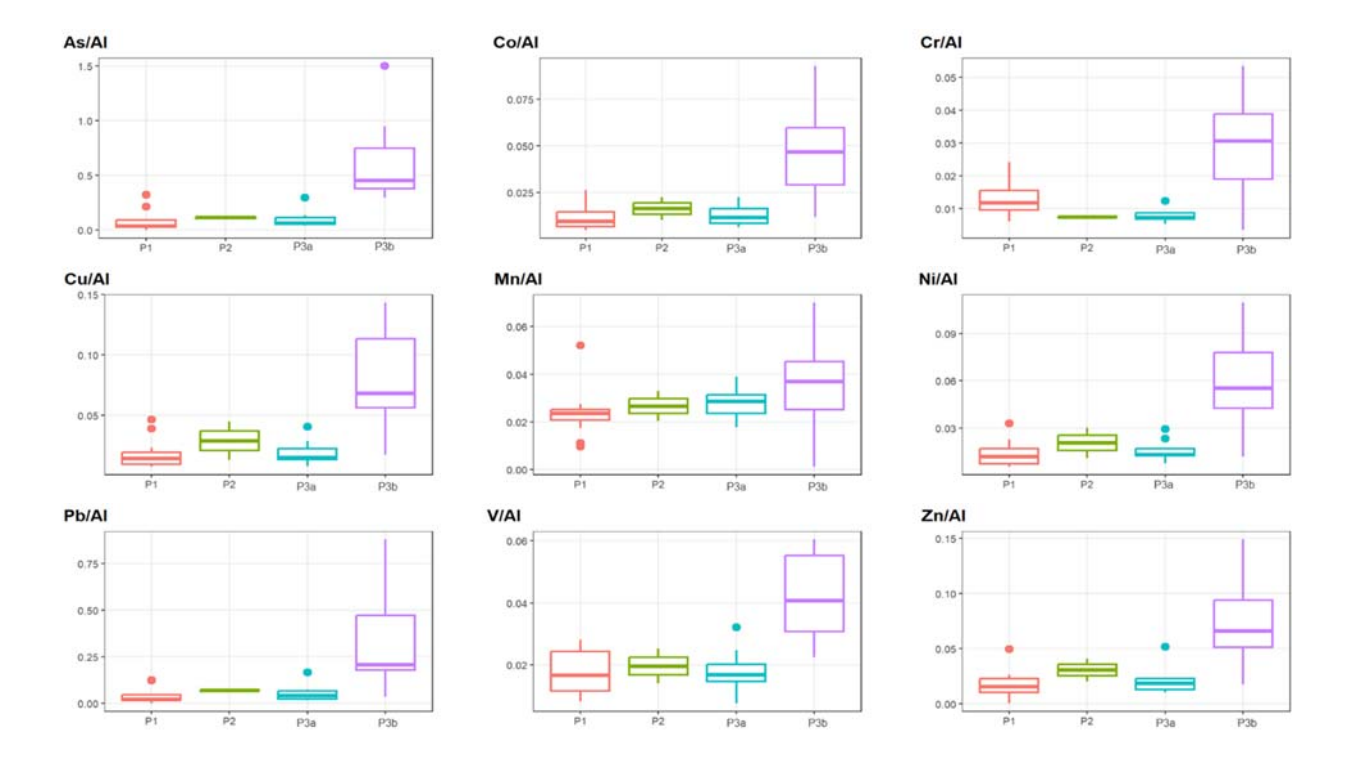


Figure S6. Time series of total particle number (cm⁻³, top) and coarse particle number concentration (bottom, cm⁻³) measured during the field campaign.

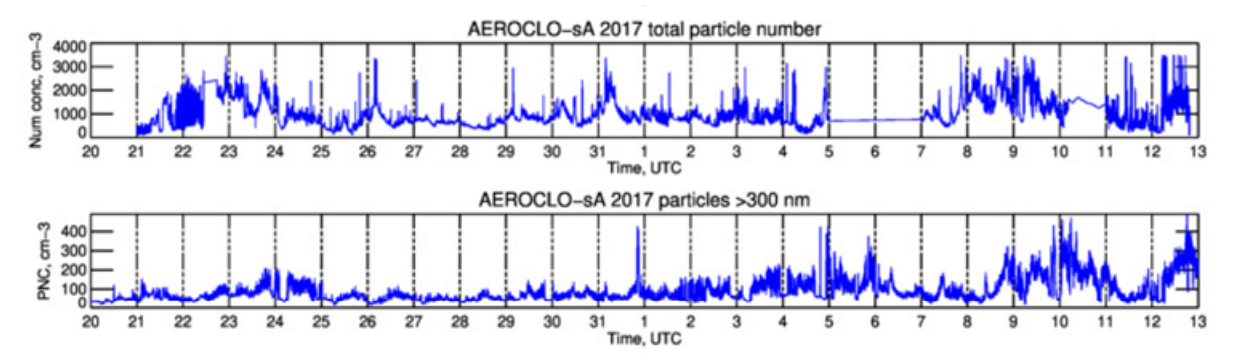
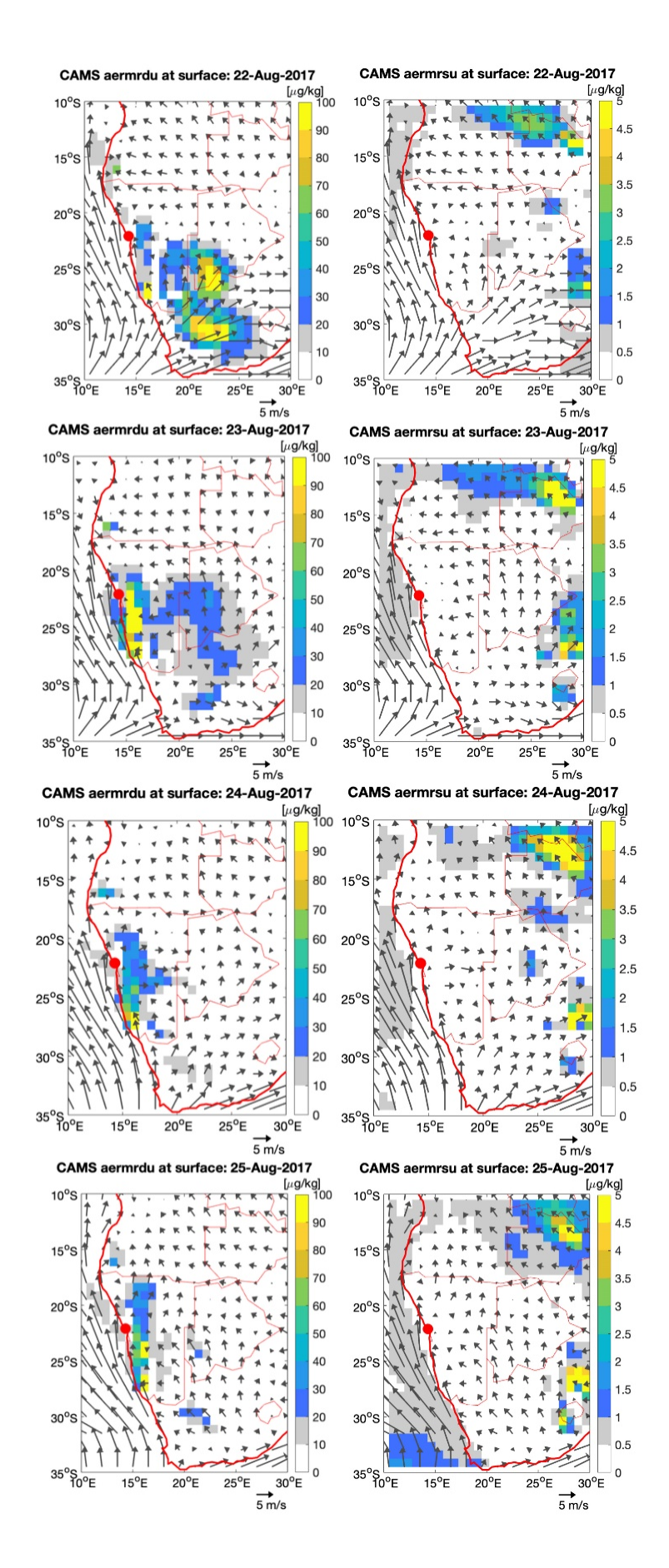
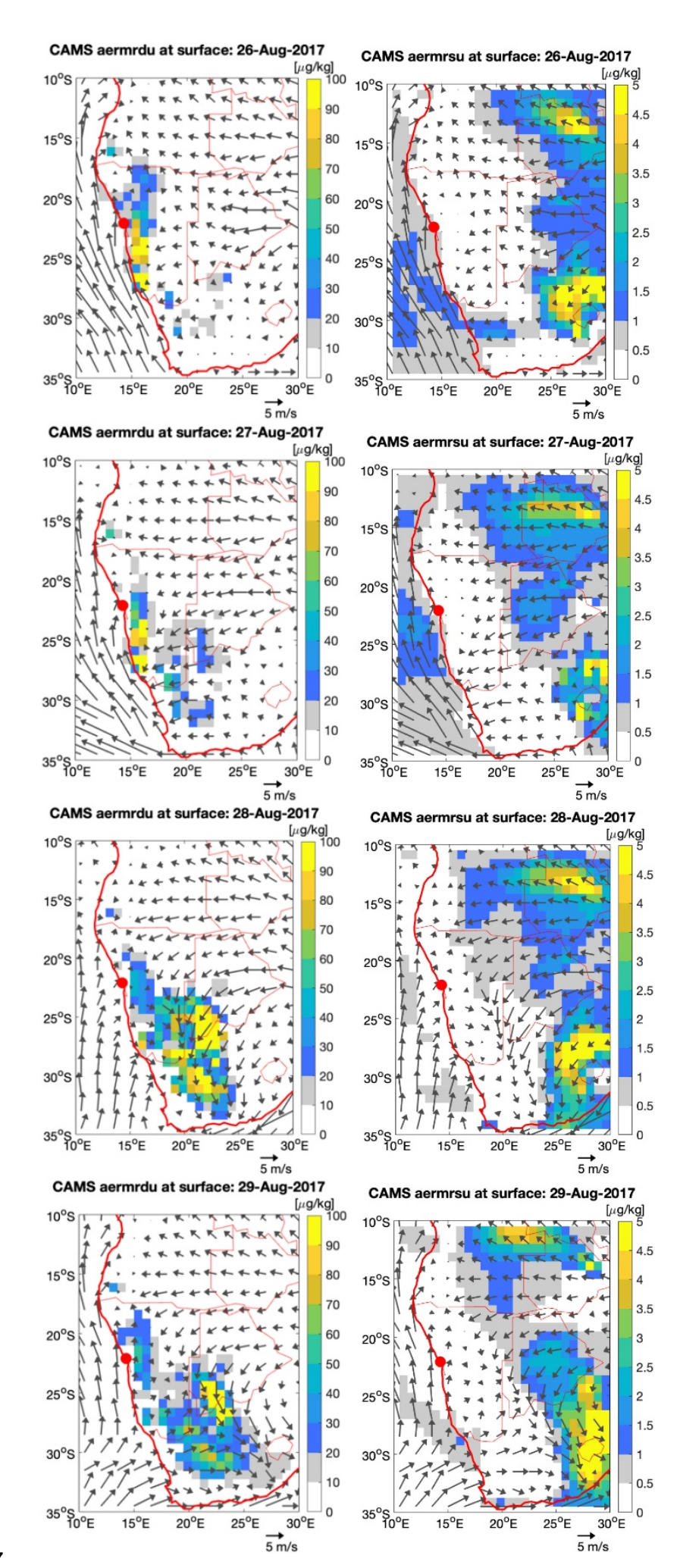
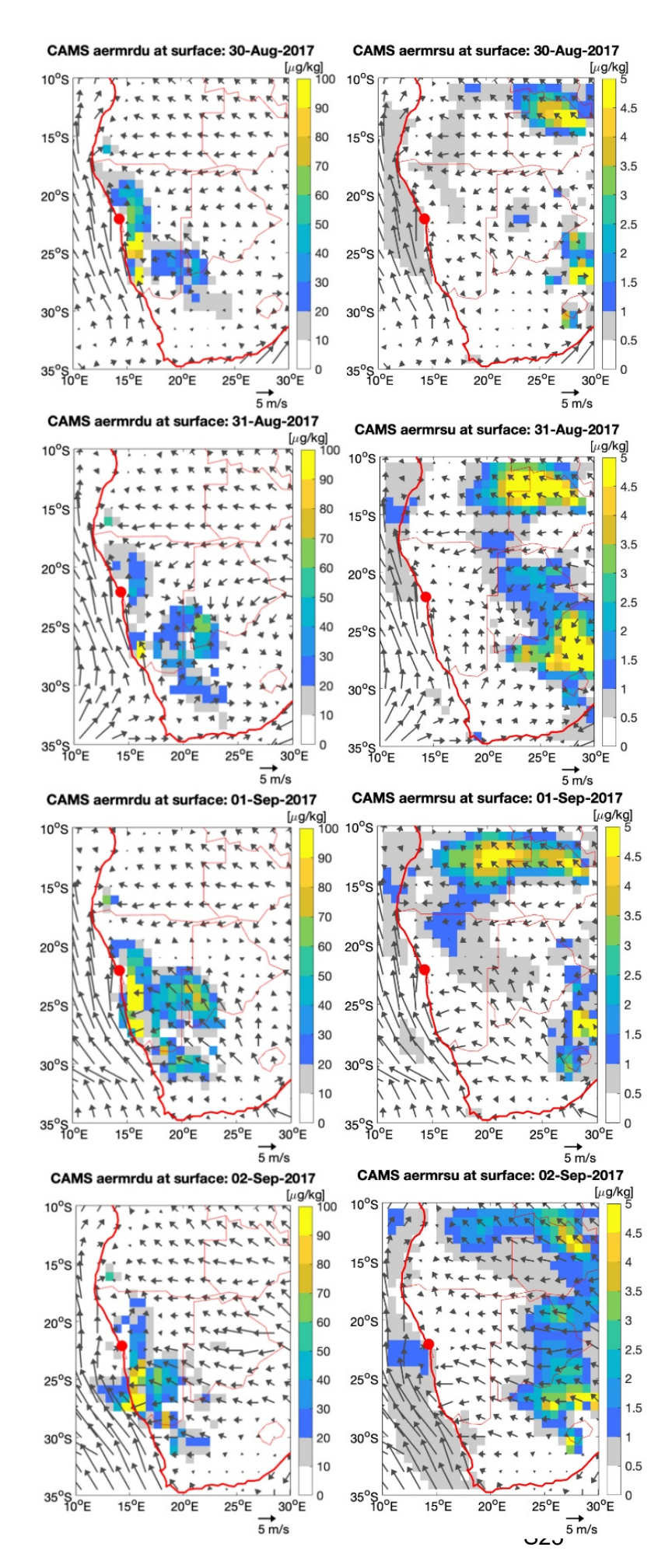
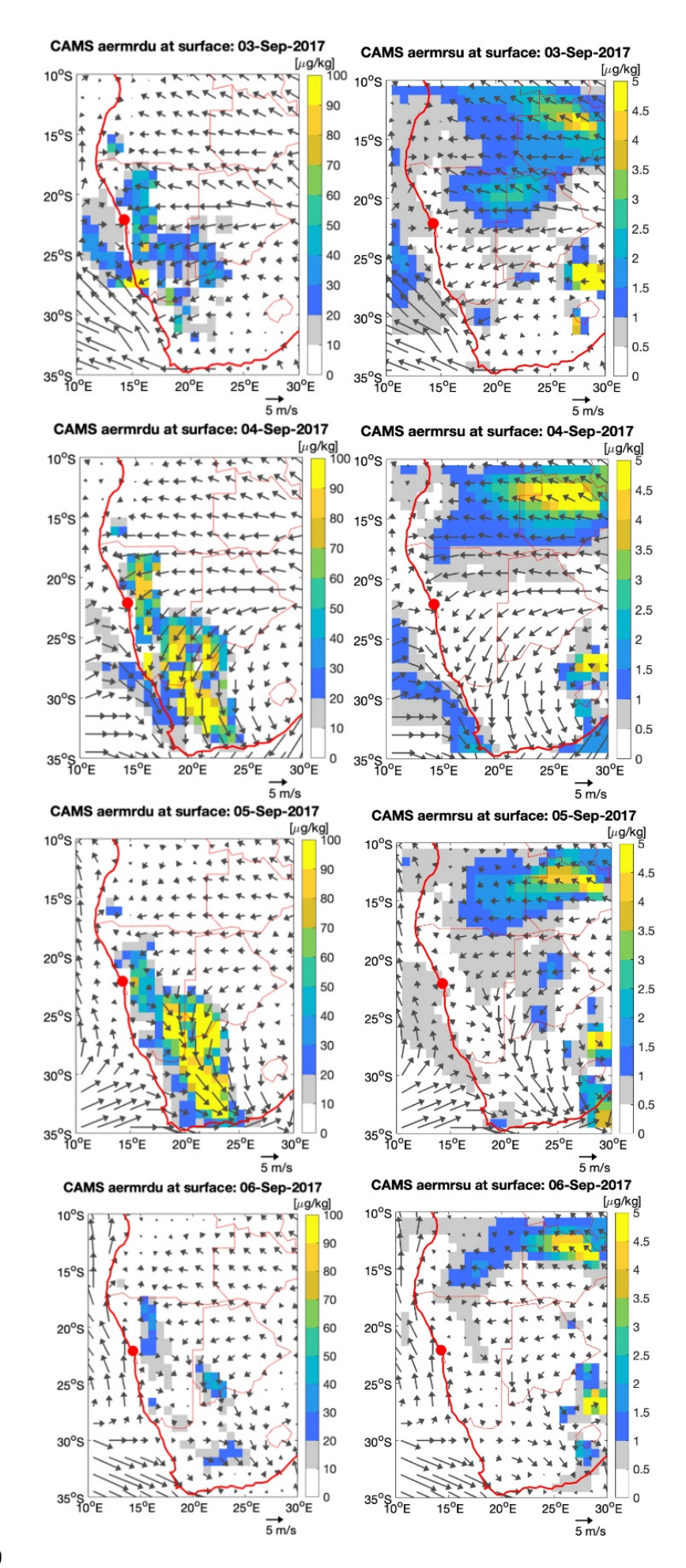


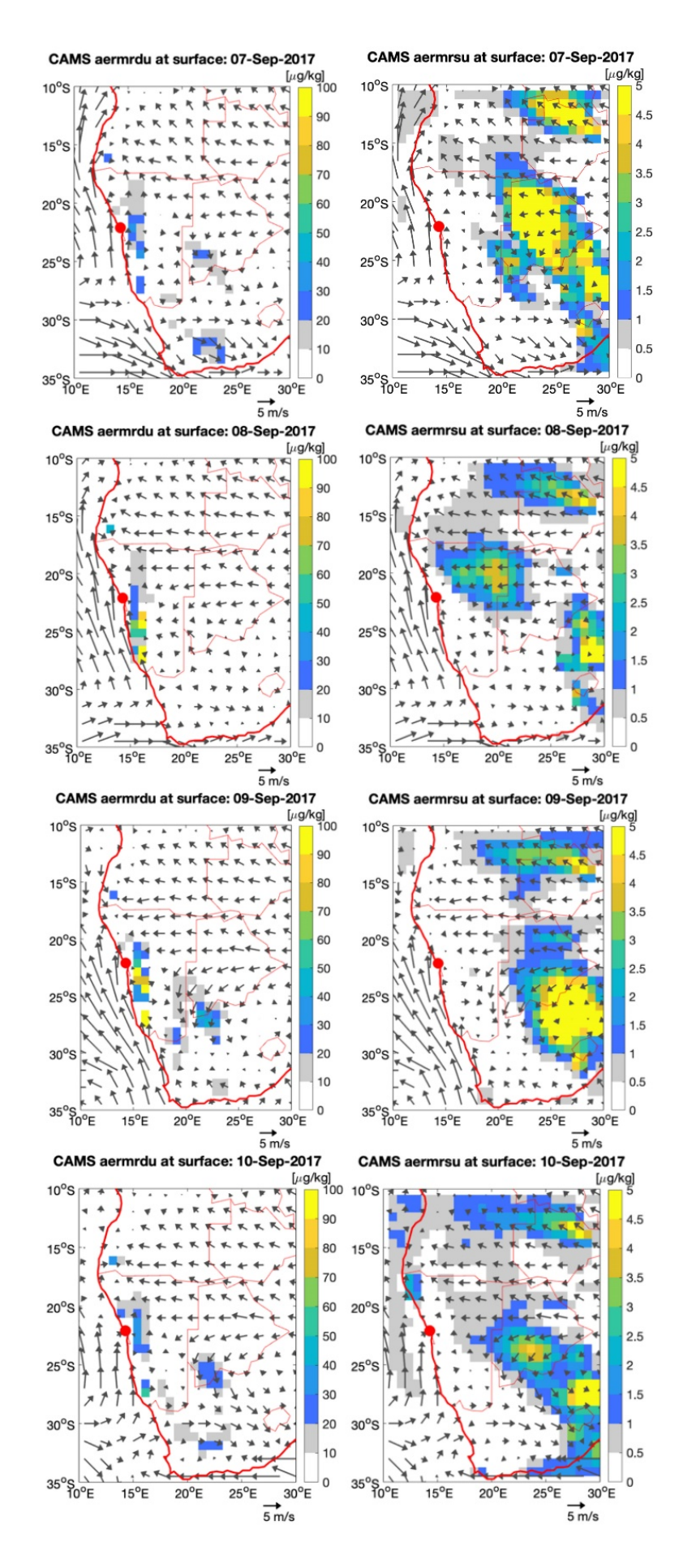
Figure S7. CAMS wind at 10-m (arrows, m s⁻¹) and surface mass mixing ratio (shading, μg kg⁻¹) for (left) mineral dust and (right) sulphate aerosols from 22 August to 12 September 2017. The red dot indicates the location of Henties Bay.











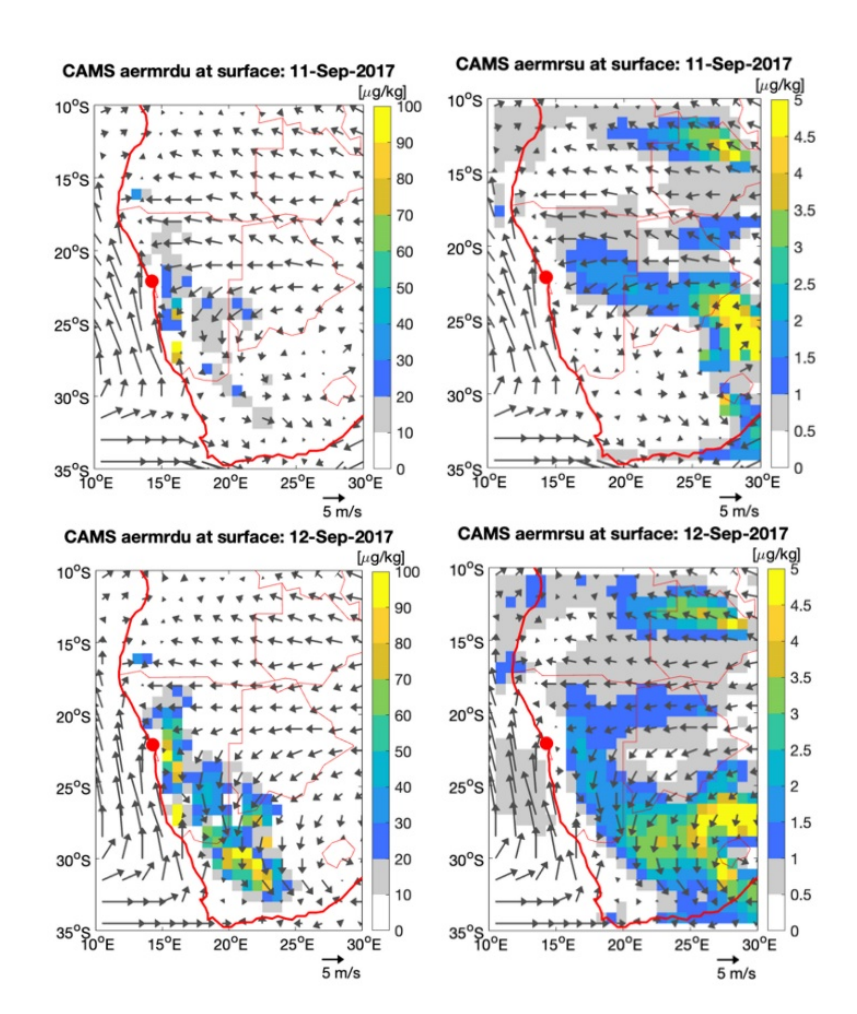
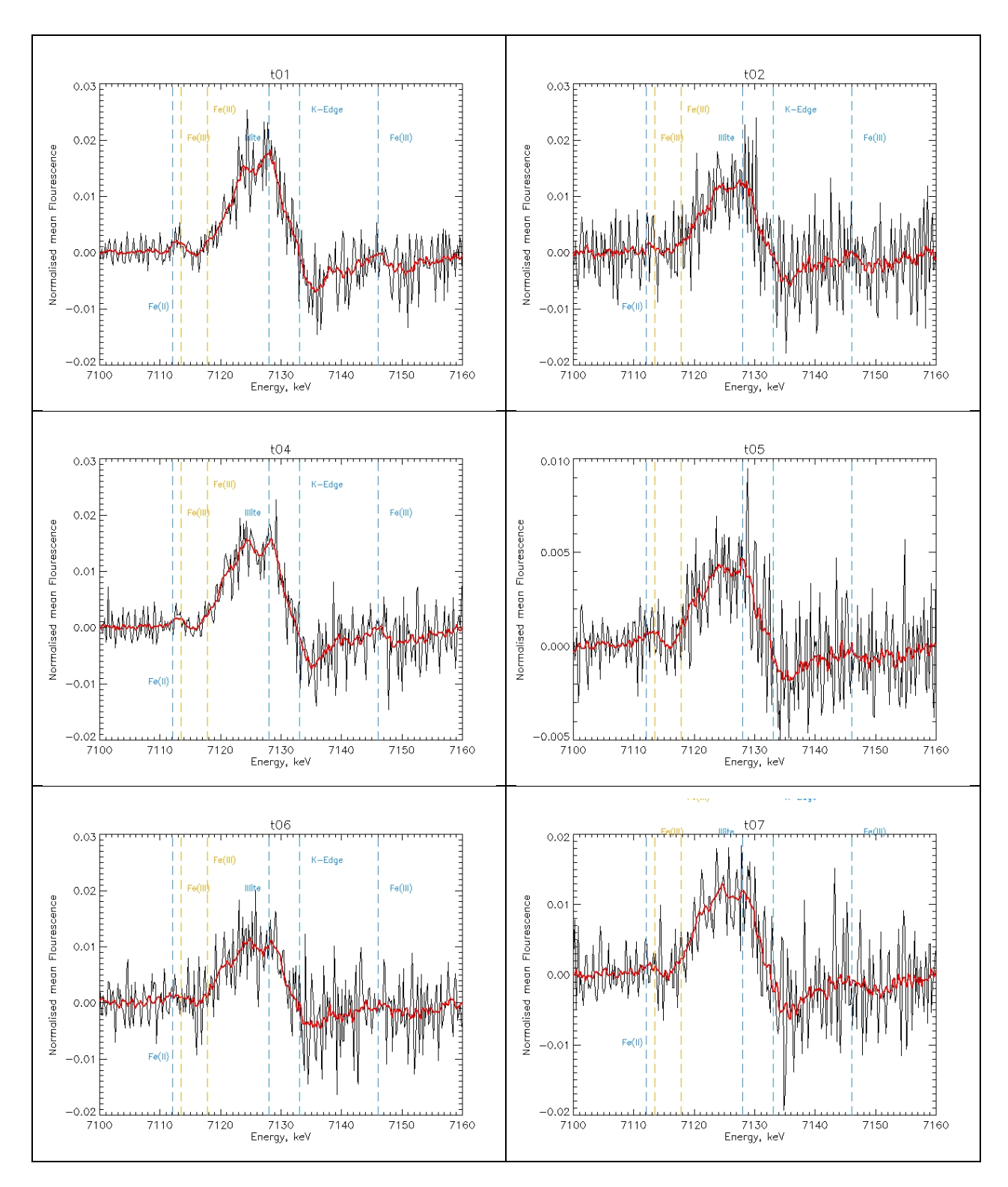
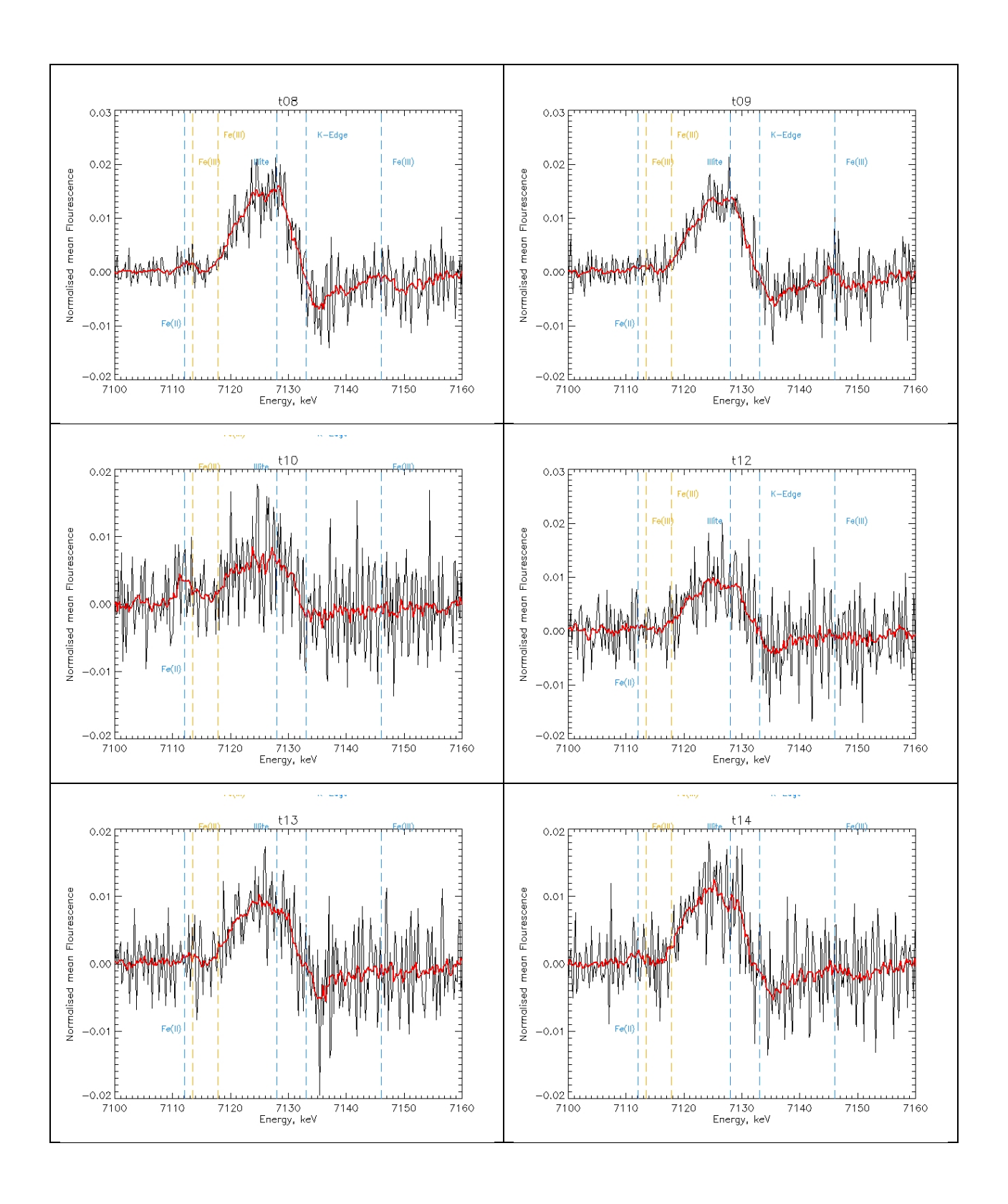
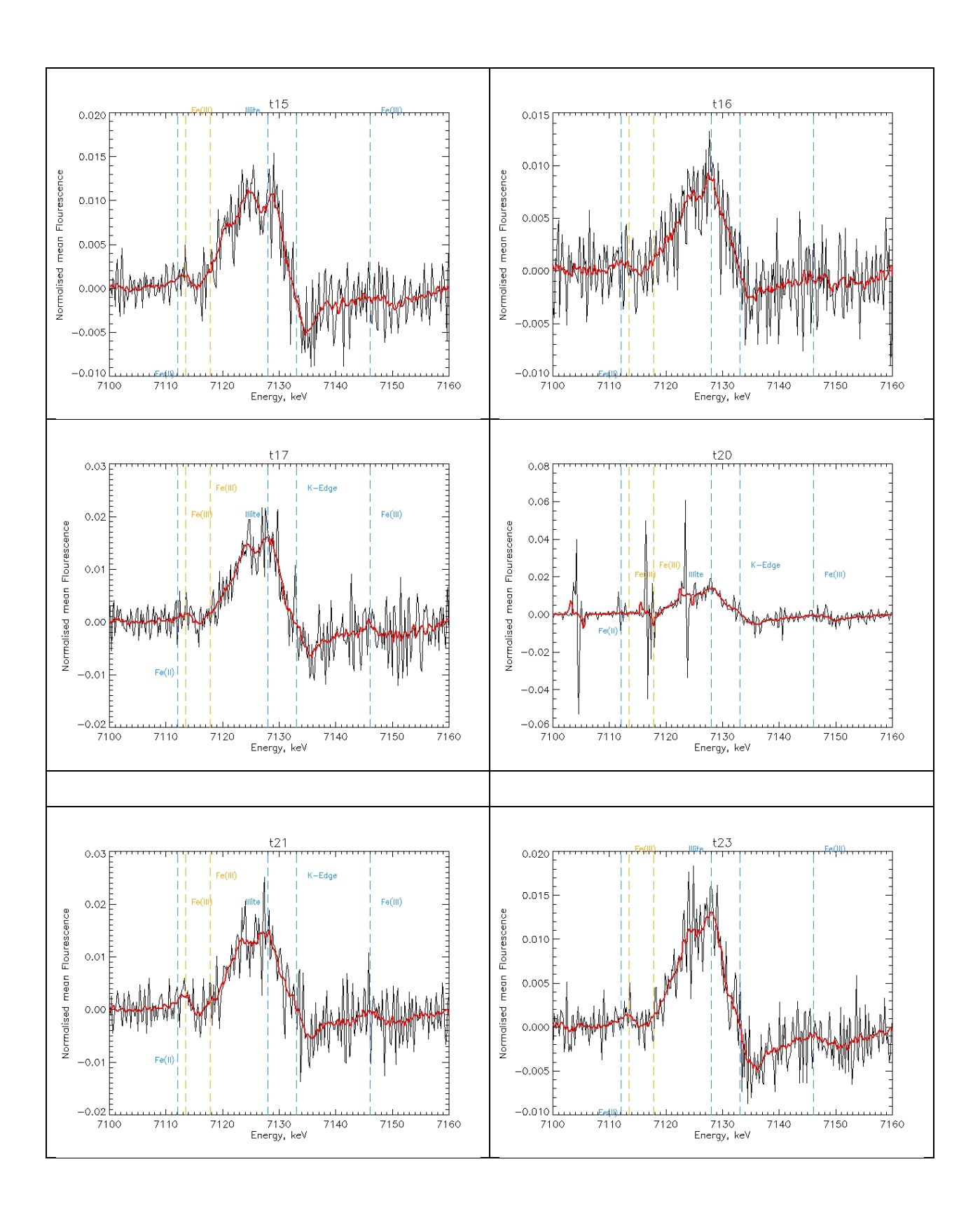
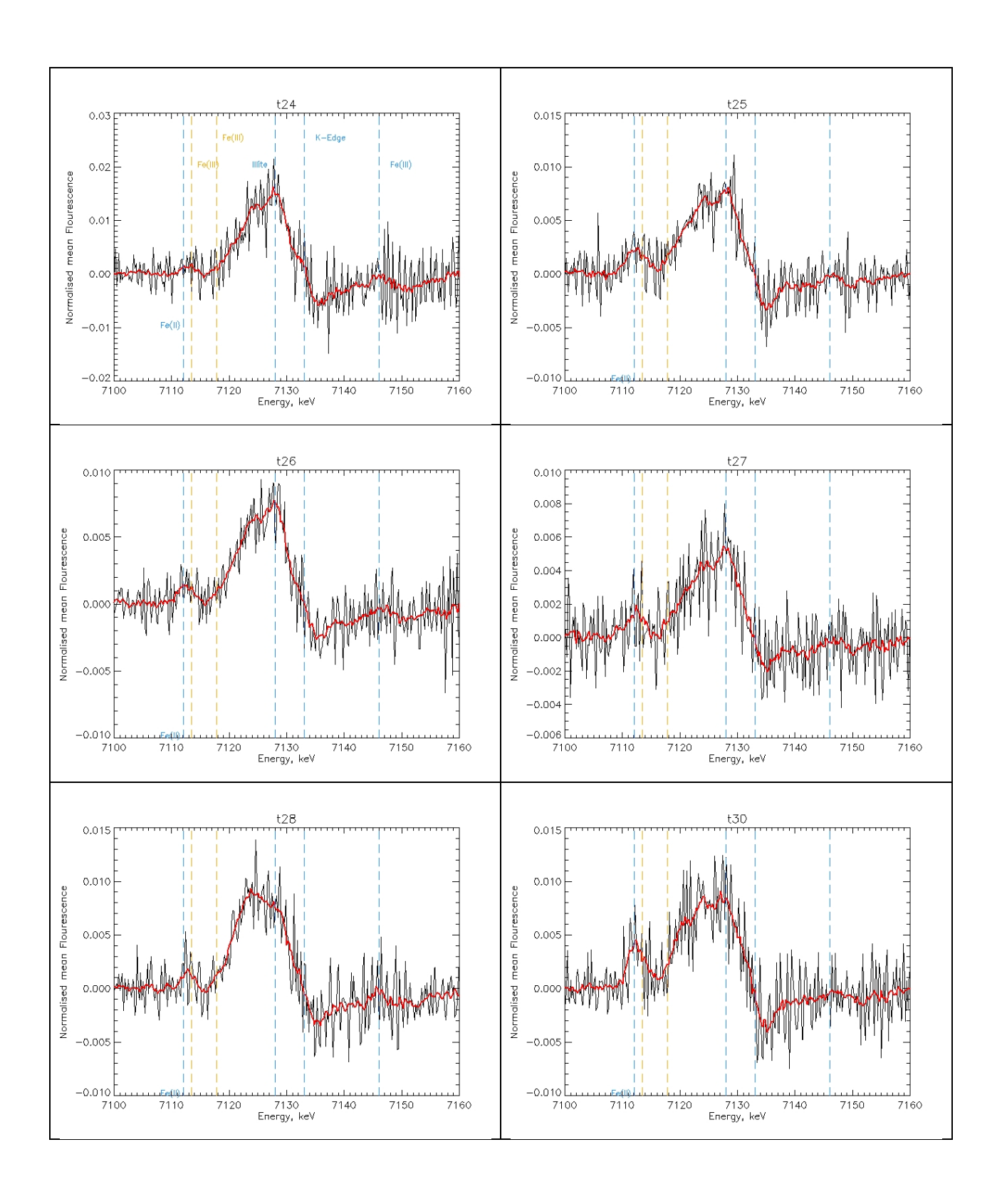


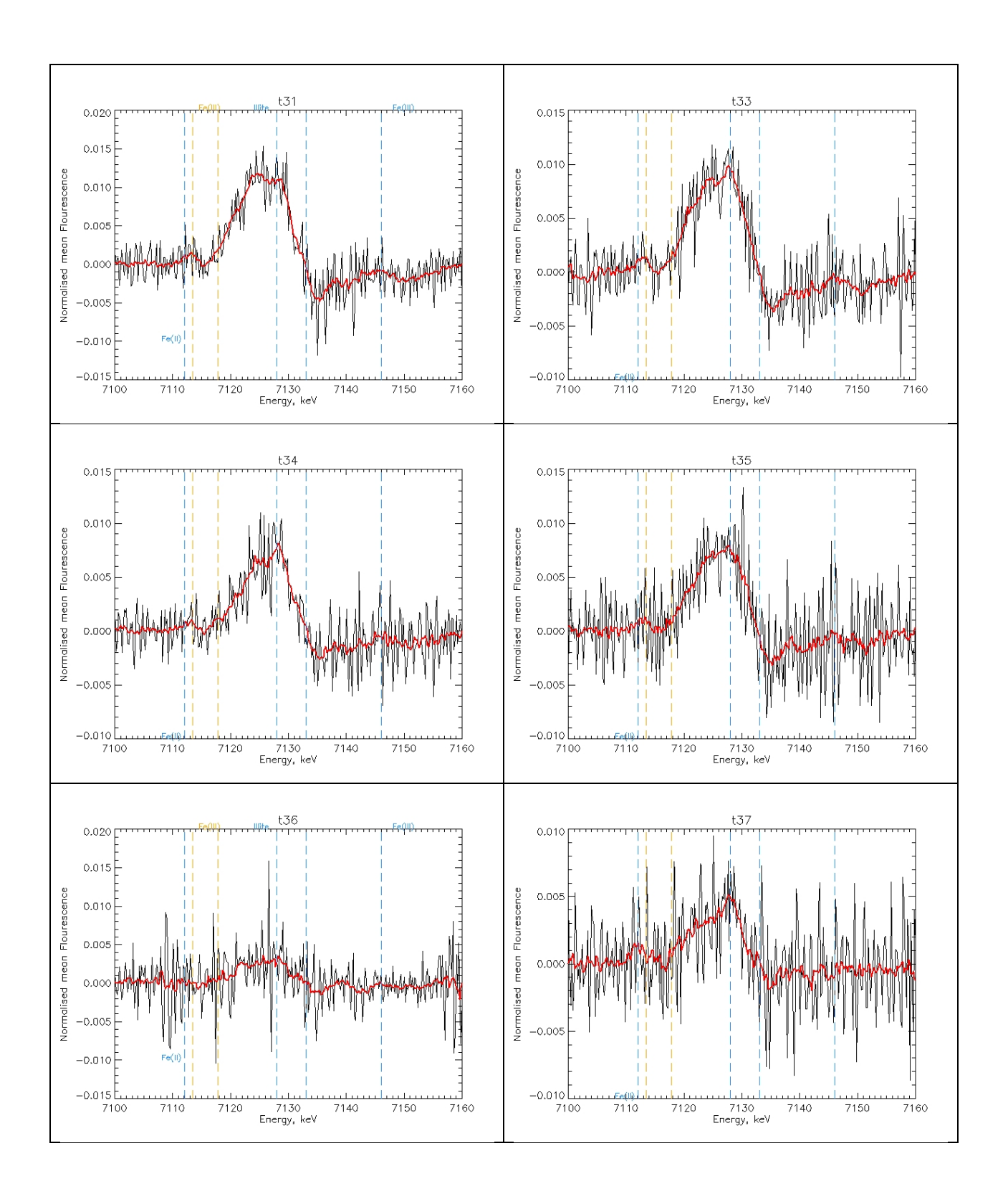
Figure S8. First derivative of the XANES normalized spectra measured during AEROCLO-sA (see Figure 5). The spectral positions of the absorption bands of Fe(II) and Fe(III) in the pre-edge region (7112.1 to 7117.8 eV) as well as those of illite (7128 eV) and various Fe(III) minerals, including hematite (7146 eV), according to Wilke et al. (2001) are indicated by vertical intermittent lines.

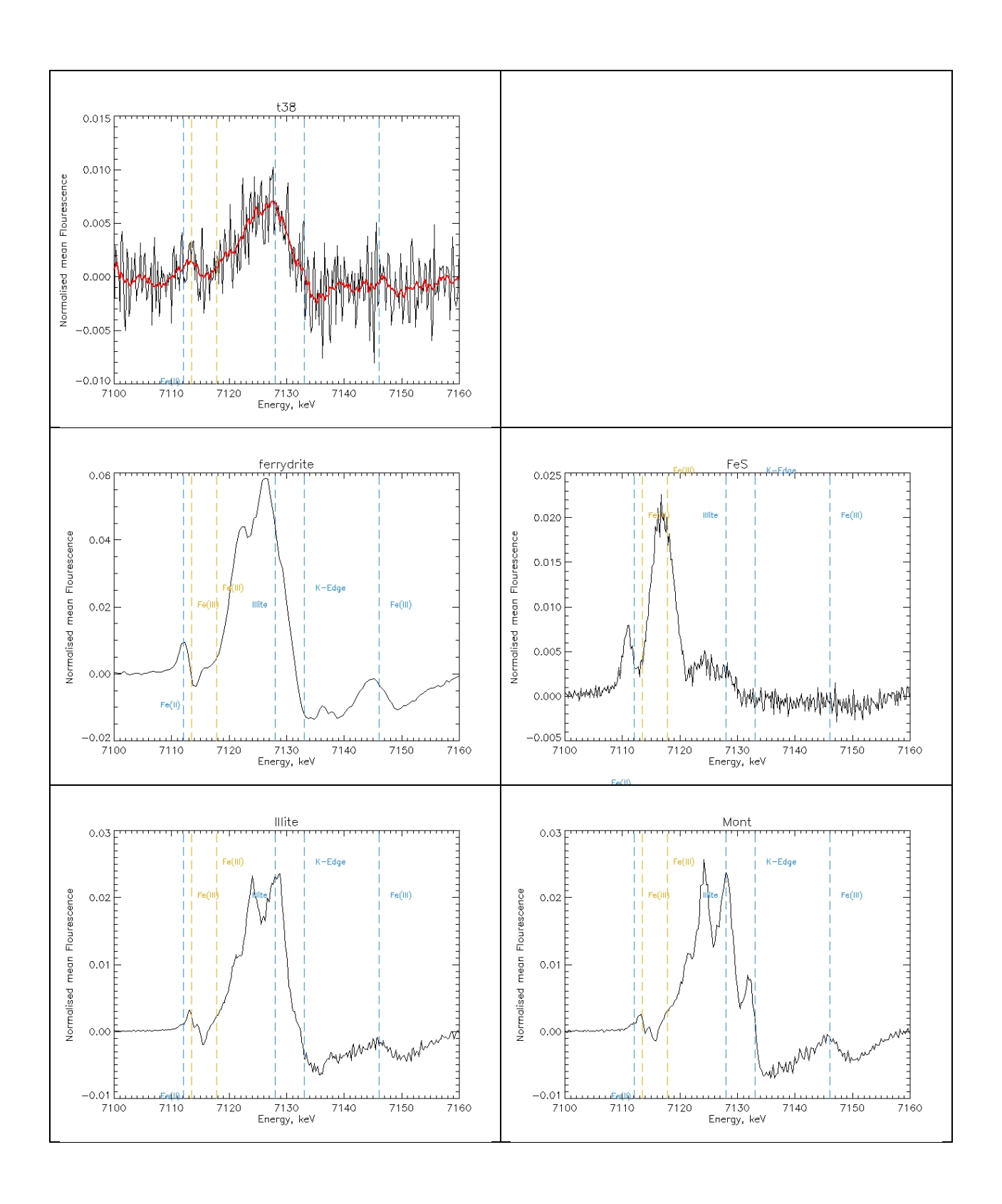


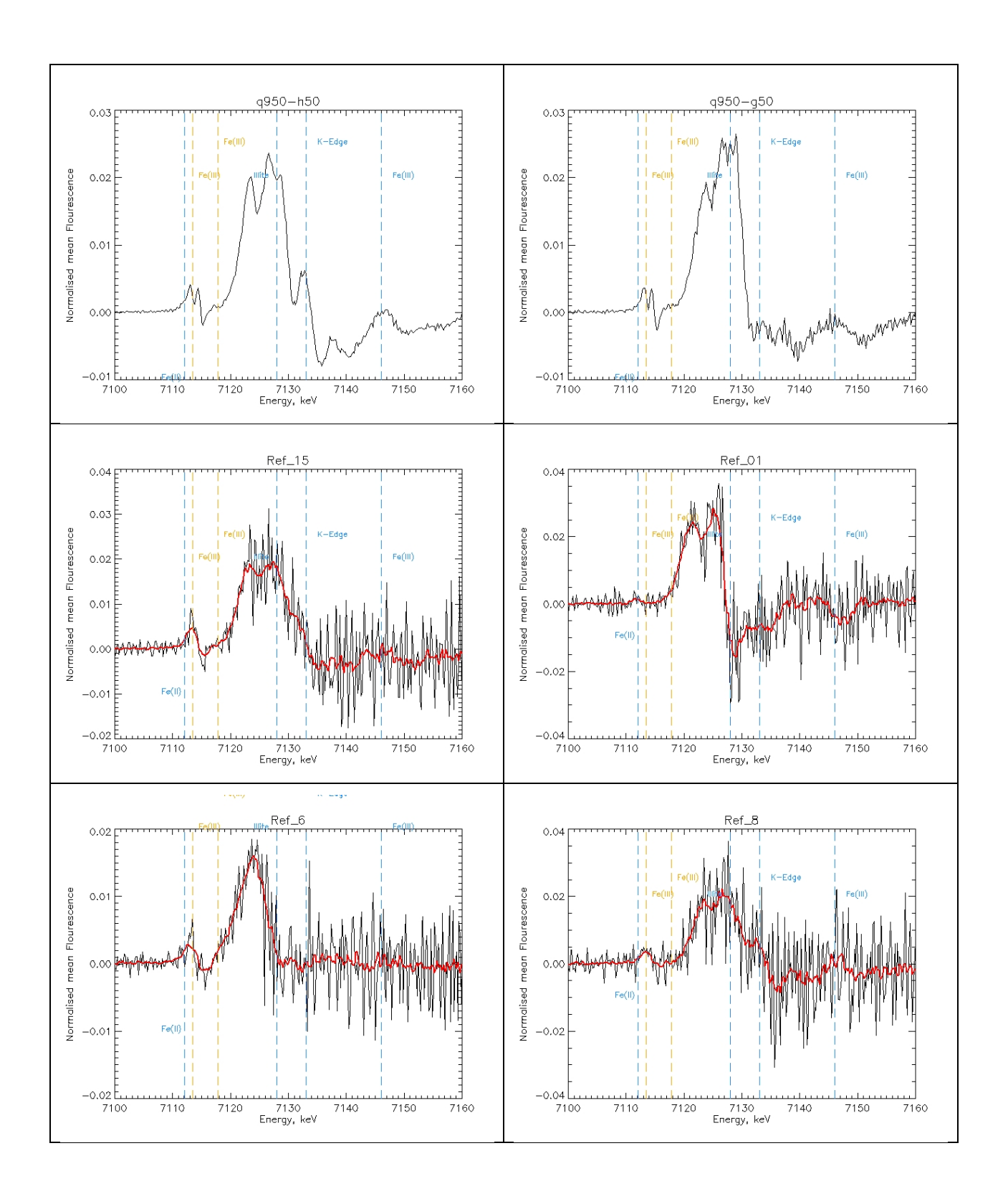












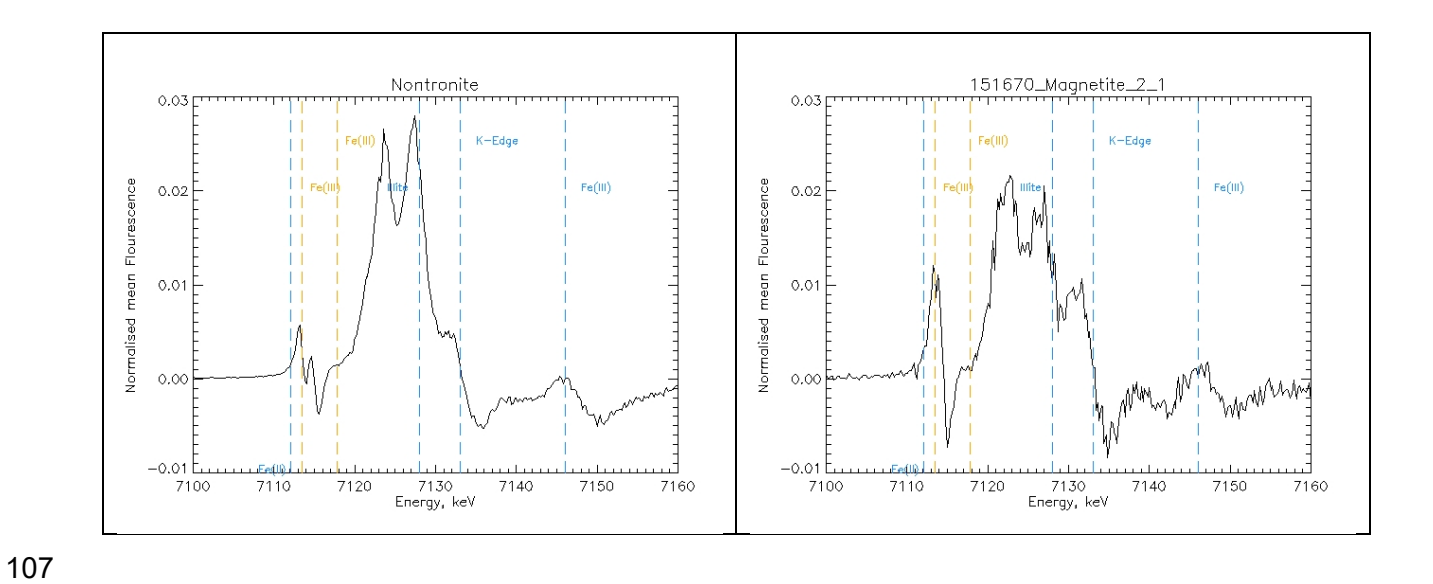
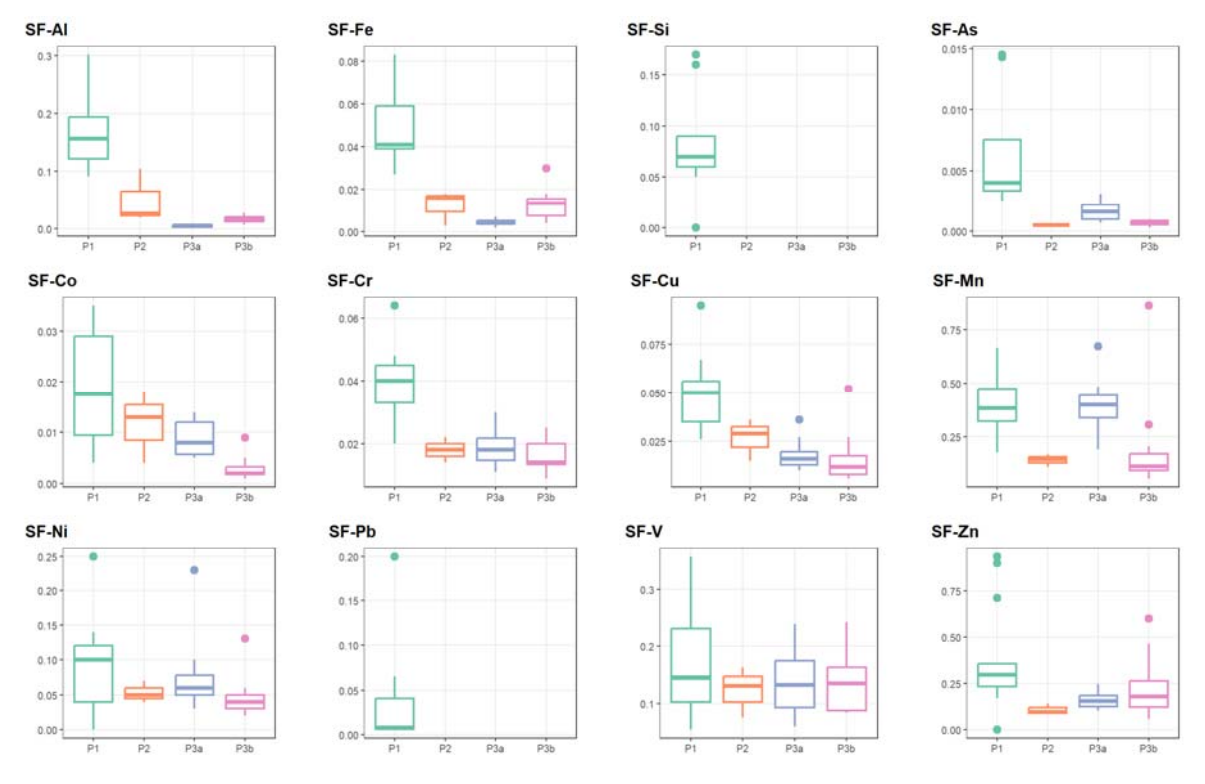


Figure S9. Box and whisker distributions of the fractional solubility of various elements during the field campaign. Values are sorted according to the meteorological periods P1 to P3. The P3 period is split into two sub-periods (P3a and P3b) to highlight the changes in the particle composition towards the end of the campaign. The box indicates the interquartile range, i.e. the 25th and 75th percentiles, and the line within the box marks the median. The whiskers indicate the quartiles 1.5 times the interquartile range. Points above and below the whiskers indicate outliers outside the 10th and 90th percentiles.



Text S1. Organic composition of aerosols

Due to low quantities of organic carbon measured during the campaign, the analysis of the composition of the organic fraction was done on extracts representing the combination of filter samples available for the P1 (T9, T12, T13 and T14), P2 (T17, T20, T21, T22, and T23) and P3 (T31, T32, T33, T38) periods. The results of formulae assignment for water soluble organic carbon (WSOC) from three samples representing a shift from P1 to P3 time ranges are depicted in Figure S10 as van Krevelen diagrams, absolute numbers, and intensity contributions of CcHhOoNnSs assignments.

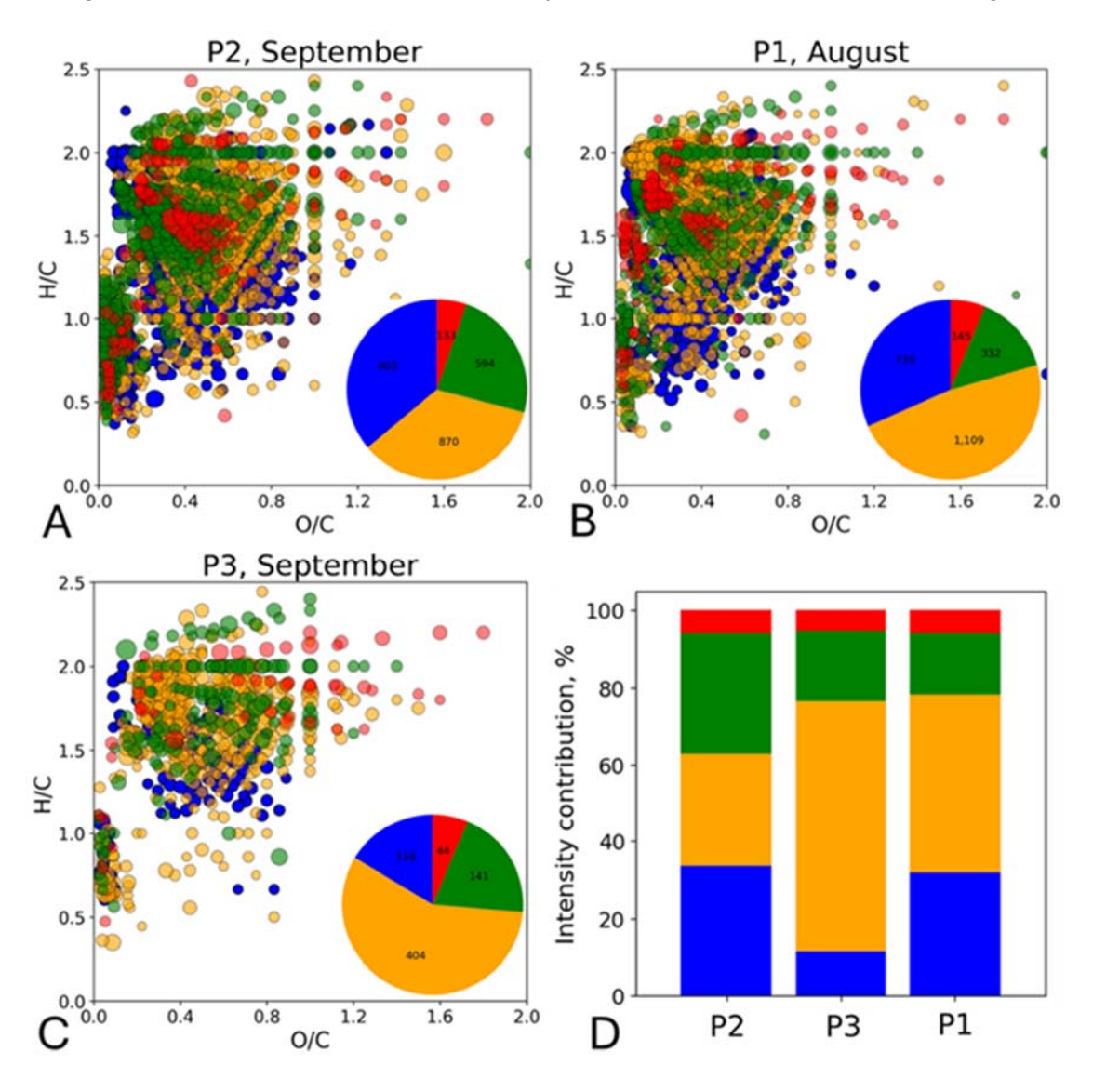


Figure S10. Van Krevelen diagrams (A, B, C) and formulae intensity contribution (D) for WSOC isolated from P1-P3 aerosols. Pie-charts indicate the number of CHO, CHON, CHOS and CHONS assignments, colour-coded in blue, orange, green and red, respectively.

A total number of 2321, 2500, and 705 molecular formulae were assigned for the P1, P2, and P3 samples, respectively, with 375 common formulae between the three. In all cases, the number of

assigned formulae per elemental group decreased in the following order: CHON>CHOS>CHONS, which is typical for organic aerosols. The number and intensity contribution of CHOS formulae were higher in P2 samples compared to other periods: 31% in P2 vs 16 and 18 in P1 and P3, respectively, with 116 common CHOS formulae between the three periods. The number of CHON formulae was highest in the P1 sample: 1109 vs. 870 and 404 for P2 and P3, respectively. At the same time intensity contribution of CHON species was highest for P3. Visual inspection of van Krevelen diagram shows the dominant contribution of saturated and unsaturated compounds with H/C > 1 in all cases.

133

134

135

136

137

138

139

140

141

142

143

144

145

146

147

148

Plotting double bond equivalent (DBE) vs molecular mass (M) diagram provides additional insights on the unique molecular features of P1, P2 and P3 periods by showing the connection between mass and unsaturation degree (Figure S11). For a deeper interpretation, the colour bar has been added designating the number of oxygen atoms in molecular formulae.

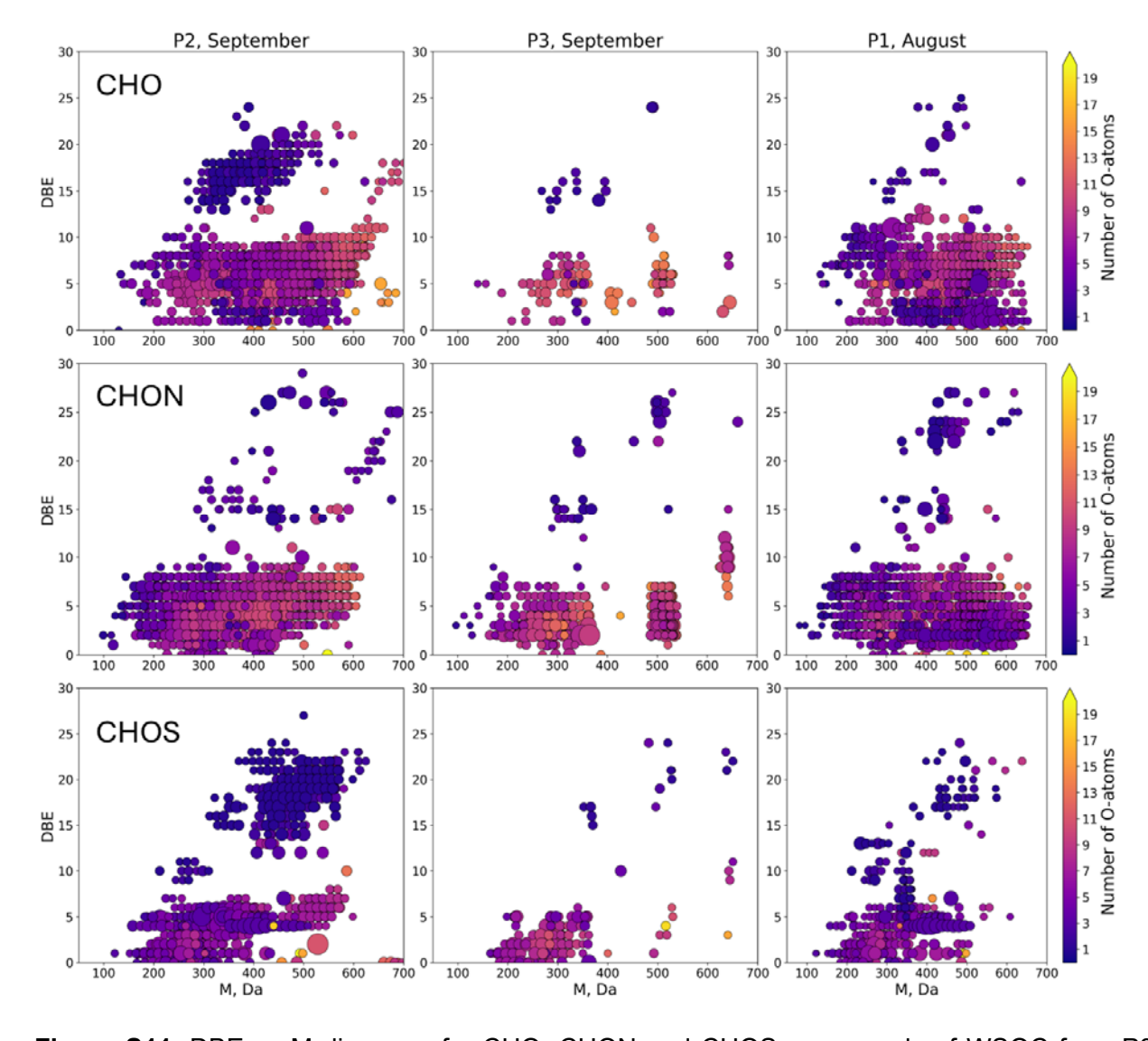


Figure S11. DBE vs M diagrams for CHO, CHON and CHOS compounds of WSOC from P3 (left panel) and P2 (right panel) samples. Color bars designate the number of oxygen atoms in molecular formulae.

150

151

152

153

154

155

156

157

158

159

160

161

162

163

164

165

166

167

168

In all cases, most of the compounds were characterized by DBE values below 10 and a mass range from 100 to 700 Da. Medium and high-molecular-weight CHO compounds with DBE below 5 were detected in all samples. Yet, in the case of P1, these compounds were low oxidized with a number of O-atoms below 5 while in the case of P2 and P3 this region of the diagram was occupied by highly oxygenated compounds. P1 sample also included highly saturated low-oxidized compounds with molecular mass around 100 Da, which were missing from P2 and P3. P1 was also distinct by the presence of high-molecular-weight low-oxidized CHON compounds. Together with CHO compounds, this likely indicates a higher contribution of biogenic emission on WSOC during P1. Peculiarity of P2 sample was in the abundance of two families of CHO and CHOS compounds clearly depicted in Figure S8. The P2 sample included middle-mass range highly unsaturated compounds with DBE > 15. In both CHO and CHOS cases, these compounds were low-oxygenated. Together with van Krevelen diagrams the observed molecular features likely indicate the increase in the contribution of burning aerosols in P2 as compared to P1 period which is aligned with the air mass origin. In addition, WSOC from P2 included relatively saturated oxidized S-containing compounds with molecular masses above 500 Da and DBE values below 10, which might indicate the contribution of sulfateenriched dust from smelting. The abrupt increase in the contribution of CHOS compounds together with the distinct appearance of new highly unsaturated compounds, supports the hypothesis on the stronger influence of anthropogenic activities on aerosol chemical composition in September.

References of supplementary material

172 Michalowicz, A., Moscovici, J., Muller-Bouvet, D., and Provost, K.: MAX: Multiplatform Applications 173 for XAFS, Journal of Physics Conference Series (Online), 190, 4, Doi:101088/1742-

174 6596/190/1/012034, 2009.

175